Transgene-free protein-based genome editing in thraustochytrids enables customizable modulation of long-chain polyunsaturated fatty acid profiles

Ishibashi, Yohei
Department of Bioscience and Biotechnology, Graduate School of Bioresource and Bioenvironmental Sciences, Kyushu University

Tanimura, Ryuji
Department of Bioscience and Biotechnology, Graduate School of Bioresource and Bioenvironmental Sciences, Kyushu University

Ataka, Yusuke
Department of Bioscience and Biotechnology, Graduate School of Bioresource and Bioenvironmental Sciences, Kyushu University

Kumagai, Akito
Department of Bioscience and Biotechnology, Graduate School of Bioresource and Bioenvironmental Sciences, Kyushu University

他

出版情報：Chemical Engineering Journal. 526, pp.171156-, 2025-12-03. Elsevier
バージョン：

Chemical Engineering Journal 526 (2025) 171156

Contents lists available at ScienceDirect

Chemical Engineering Journal

journal homepage: www.elsevier.com/locate/cej

Transgene-free protein-based genome editing in thraustochytrids enables customizable modulation of long-chain polyunsaturated fatty acid profiles

Yohei Ishibashi [a,*], Ryuji Tanimura [a], Yusuke Ataka [a], Akito Kumagai [a], Daiske Honda [b], Makoto Ito [a], Nozomu Okino [a]

[a] Department of Bioscience and Biotechnology, Graduate School of Bioresource and Bioenvironmental Sciences, Kyushu University, 744 Moto-oka, Nishi-ku, Fukuoka, 819-0395, Japan

[b] Department of Biology, Faculty of Science and Engineering, Konan University, Hyogo 658-8501, Japan

ARTICLE INFO

Keywords:
Cas9
Desaturase
Elongase
LC-PUFA
Metabolic engineering
Thraustochytrid
Transgene-free genome editing

ABSTRACT

Long-chain polyunsaturated fatty acids (LC-PUFAs), such as docosahexaenoic acid (DHA) and eicosapentaenoic acid (EPA), are essential lipids with significant health benefits. The functional properties of LC-PUFAs are influenced by carbon chain length, degree of unsaturation, and the position of unsaturated bonds within the molecule. *Parietichytrium*, a genus of the thraustochytrids, is a marine oleaginous microorganism that possesses a complete set of elongase (ELO) and desaturase (DES) genes required for DHA biosynthesis. Targeted disruption of specific ELO or DES genes using heterologous antibiotic resistance markers enabled modulation of the DHA biosynthetic pathway, thereby facilitating the production of structurally diverse LC-PUFAs. In this study, we developed a transgene-free CRISPR-Cas9 genome editing platform utilizing ribonucleoprotein (RNP) complex, applicable to three phylogenetically distinct thraustochytrid genera: *Aurantiochytrium limacinum* ATCC MYA-1381, *Thraustochytrium aureum* ATCC 34304, and *Parietichytrium sarkarianum* SEK364. We applied it to disrupt three key genes, *Δ4DES, C20ELO,* and *Δ5DES*, involved in DHA biosynthesis of *P. sarkarianum* SEK364. Δ4DES disruption abolished DHA and n-6 docosapentaenoic acid (n-6DPA) production, resulting in the accumulation of n-3DPA and docosatetraenoic acid (DTA). C20ELO deletion led to predominant accumulation of EPA and arachidonic acid (ARA). Notably, the Δ5DES KO strain exhibited significant accumulation of eicosatetraenoic acid (ETA) and dihomo-γ-linolenic acid (DGLA). Optimization of culture conditions further enhanced their production without growth defects. These findings demonstrate the feasibility of RNP-mediated genome editing in thraustochytrids and highlight the potential of genome-edited *Parietichytrium* strains as versatile, transgene-free platforms for the tailored biosynthesis of diverse LC-PUFAs.

1. Introduction

Long chain polyunsaturated fatty acids (LC-PUFAs) are defined as fatty acids with more than twenty carbon chains, and with more than two unsaturated bonds of the cis-configuration separated by a single methylene group. Furthermore, LC-PUFAs are categorized as either n-3 or n-6 based on the position of the unsaturated bond in relation to the terminal methyl end [1]. Docosahexaenoic acid (DHA, C22:6n-3) and eicosapentaenoic acid (EPA, C20:5n-3) are known as beneficial n-3LC-PUFAs used as supplements and medicines [2]. LC-PUFAs have different physiological functions in humans depending on the carbon chain length and number of unsaturated bonds. DHA is a prevalent component of the retina and brain, contributing to their function and development [3]. The incidence of renal disease, such as age-related macular degeneration and central geographic atrophy, was lower in individuals with high DHA intake [4,5], suggesting the significance of sufficient dietary levels of DHA for retinal stability. The purified ethyl ester form of EPA has been approved as a therapeutic agent for obstructive arteriosclerosis and hypertriglyceridemia [6]. n-3 docosapentaenoic acid (n-3DPA, C22:5n-3), an intermediate product in the conversion process from EPA to DHA, is expected to have unique health benefits, including improvements in plasma lipid parameters [7], platelet aggregation [8], and insulin sensitivity [9]. A recent study demonstrated that dihomo-γ-linolenic acid (DGLA, C20:3n-6) is a requisite factor in the initiation of autonomic repair in the brain following ischaemic stroke [10]. The oral administration of DGLA mice with cerebral infarction resulted in an

* Corresponding author.
E-mail address: ishibashiyo@agr.kyushu-u.ac.jp (Y. Ishibashi).

https://doi.org/10.1016/j.cej.2025.171156
Received 6 August 2025; Received in revised form 20 October 2025; Accepted 21 November 2025
Available online 28 November 2025

improvement in neurological symptoms and a reduction in cerebral infarct volume following a stroke. The rapid aging of the global population is expected to significantly impact the prevalence of geriatric diseases, leading to a sharp increase in the number of affected patients worldwide. LC-PUFAs are efficacious interventions in the prevention of such diseases, consequently leading to an increase in demand.

DHA and EPA are industrially produced from fish oil, although the primary producers of LC-PUFAs are mainly marine microalgae and heterotrophic microorganisms [11]. Abundance and community structure of marine primary producers of n-3 LC-PUFA are highly sensitive to changes in environmental parameters. Thus, the increase in water temperature and ocean acidification caused by climate change adversely affects the content and composition of fatty acids in marine primary producers, reducing the availability of natural n-3 LC-PUFA [11]. Since the supply of n-3 LC-PUFAs will be insufficient in the future, sustainable and alternative sources of n-3 LC-PUFAs are urgently required. Thraustochytrids are eukaryotic marine protists, including the typical genera *Aurantiochytrium*, *Aplanochytrium*, *Schizochytrium*, *Thraustochytrium*, and *Parietichytrium*, which belong to the Stramenopiles, class Labyrinthulomycetes, family Thraustochytriaceae [12,13]. Thraustochytrids have recently received increasing attention from academic as well as industrial fields because they produce huge amounts of DHA. Several studies have explored genetic engineering approaches to enhance DHA productivity in thraustochytrids [14–18]. Although thraustochytrids are considered promising alternative sources of LC-PUFAs, one of the major limitations is their low or negligible productivity of n-3 LC-PUFAs other than DHA [19]. In particular, the biosynthesis of EPA, a highly valuable n-3 LC-PUFA, remains inefficient, and recent efforts have focused on improving its productivity through metabolic engineering [20].

Aurantiochytrium, formerly classified as *Schizochytrium,* synthesizes DHA using malonyl-CoA as an elongation substrate via PUFA synthase (PUFA-S), which is composed of multiple subunits containing multiple catalytic domains [12,21,22]. PUFA-S is an efficient system for the anaerobic synthesis of DHA; however, it is unable to produce other useful LC-PUFAs, such as EPA or n-3DPA. On the other hand, *Parietichytrium* has PUFA-S independent aerobic DHA synthesis pathway composed of several elongases (ELOs) and desaturases (DESs) (ELO/DES pathway) [23]. Importantly, EPA and n-3DPA-producing *Parietichytrium* could be generated by disrupting C20ELO and Δ4DES, respectively. The former converts EPA (C20:5) to n-3DPA (C22:5), and the latter converts n-3DPA (C22:5) to DHA (C22:6). These results indicate that the desired LC-PUFA can be produced in *Parietichytrium* by the modulation of the ELO/DES pathway [23]. However, these modified strains are classified as genetically modified organisms (GMOs), because they were developed through gene targeting utilizing heterologous antibiotic resistance genes as selection markers. The application of GMO-thraustochytrids in food or dietary supplements remains challenging due to the stringent and protracted regulatory approval processes required for the commercial use of GMOs in some countries, including Japan [24]. Moreover, the strains established in our previous study had exhausted all available antibiotic resistance genes as selectable markers, preventing further genetic modifications and thereby limiting strategies to improve LC-PUFA productivity. This constraint underscores the need for novel genetic engineering approaches that are not restricted by the number of selectable markers.

CRISPR/Cas9 is a genome-editing tool derived from a bacterial immune system, allowing precise and targeted modifications to genomic DNA [25]. The CRISPR component functions as a guide that directs the Cas9 nuclease to a specific genomic location. Once guided to the target sequence by the CRISPR RNA (crRNA) and the trans-activating CRISPR RNA (tracrRNA), the Cas9 protein induces a double-strand break in the genomic DNA, allowing for gene insertions, deletions, or corrections through cellular repair mechanisms. Direct delivery of Cas9 as a ribonucleoprotein (RNP) complex, comprising crRNA and tracrRNA, into cells circumvents the integration of transgenes into the host genome [26]. Furthermore, this strategy facilitates transient gene editing without permanent genomic modifications, thereby minimizing the potential for off-target effects. Therefore, the RNP-based approach has emerged as a reliable and efficient method for deletion-type genome editing applications that are not classified as GMO in many countries, including Japan, India, the United States, Canada, Australia, and several South American nations [27]. To date, two studies have reported the application of CRISPR/Cas9 in *Aurantiochytrium* (*Schizochytrium*). Watanabe et al. demonstrated that the use of RNP together with donor constructs improves homologous recombination efficiency [28], whereas Duan et al. developed an innovative gRNA expression system driven by an endogenous $tRNA^{Gly}$-based Pol III promoter, achieving efficient genome editing [29]. However, both approaches rely on antibiotic resistance genes as selectable markers in either donor construct for homologous recombination or gRNA/Cas9 expression constructs, and have not yet enabled the isolation of genome-edited strains using RNPs alone.

In this study, we evaluated the feasibility of genome editing in thraustochytrids by directly introducing RNPs without using selection markers. Initially, the β-glucuronidase (GUS) gene, a color selection marker, was introduced into *Aurantiochytrium limacinum* ATCC MYA-1381, a representative strain of thraustochytrids, [30]. RNPs containing crRNAs targeting GUS were prepared, and RNP transfection conditions and genome editing efficiency were verified using colony color as an indicator. Genome editing was successfully demonstrated not only in *A. limacinum* ATCC MYA-1381 but also in *Thraustochytrium aureum* ATCC 34304, indicating that the method the method is not restricted to a single genus within thraustochytrids. We applied this method to disrupt the *Δ4DES* and *C20ELO* genes in *Parietichytrium sarkarianum* SEK364 to establish transgene-free strains capable of producing EPA and n-3DPA, respectively. Additionally, we successfully developed a *Δ5 desaturase* (*Δ5DES*) genome-edited strain with high DGLA and eicosatetraenoic acid (ETA) production capacity. This study demonstrates that gene knockout in thraustochytrids can be achieved without the use of transgenes such as selection markers, enabling targeted modification of LC-PUFA profiles in *P. sarkarianum* SEK364.

2. Materials and methods

2.1. Strains and culture

Aurantiochytrium limacinum ATCC MYA-1381 and *Thraustochytrium aureum* ATCC 34304 were obtained from American Type Culture Collection (VA, USA). *Parietichytrium sarkarianum* SEK364 was isolated from seawater of the Iriomote Islands in Okinawa, Japan [13]. *A. limacinum* ATCC MYA-1381, *T. aureum* ATCC 34304, *P. sarkarianum* SEK364, and genome edited mutants derived from these parental strains were grown in GY medium [3 % glucose and 1 % yeast extract in 1.75 % artificial seawater (SEALIFE, Nihonkaisui Co.)] supplemented with 0.1 % vitamin mixture (0.2 % vitamin B_1, 0.001 % vitamin B_2, and 0.001 % vitamin B_{12}) and 0.2 % trace element mixture (3 % EDTA di-sodium, 0.15 % $FeCl_3{\cdot}6H_2O$, 3.4 % H_3BO_4, 0.43 % $MnCl_2{\cdot}4H_2O$, 0.13 % $ZnSO_4{\cdot}7H_2O$, 0.026 % $CoCl_2{\cdot}6H_2O$, 0.026 % $NiSO_4{\cdot}6H_2O$, 0.001 % $CuSO_4{\cdot}5H_2O$, and 0.0025 % $Na_2MoO_4{\cdot}2H_2O$) at 25 °C with rotation at 150 rpm for the period indicated. Potato dextrose agar (PDA) plate (50 % potato dextrose, 1.75 % artificial sea water, 2 % agar) supplemented with vitamin and trace element mixture was used for plate culture. Cell growth was monitored by measuring dry cell weight (DCW) or optical density (OD) at 600 nm (OD_{600}). The glucose concentration of the culture medium was measured by the Glucose CII test (FUJIFILM Wako Pure Chemical Co.). WT and genome-edited mutants of *P. sarkarianum* SEK364 were cultured in GY medium supplemented with either 3 % or 6 % glucose, or at 25 °C or 18 °C to optimize culture conditions to improve their LC-PUFA productivity. SILICOSEN®, air-permeable silicone rubber plugs, was purchased from Shin-Etsu Polymer Co., Ltd. To evaluate the phenotypic stability of genome-edited strains, OD_{600} was measured

every four days. Cultures were serially transferred into 3 mL of GY medium at an initial OD_{600} of 0.1. At each transfer, 1 mL of culture was collected for the assessment of LC-PUFA composition and productivity. We repeated this subculturing procedure four times to evaluate the stability of the genome-edited strains.

2.2. Generation of GUS-expressing strains

To enable β-glucuronidase (GUS) expression in *A. limacinum* ATCC MYA-1381 and *T. aureum* ATCC 34304, a codon-optimized GUS gene was artificially synthesized (Eurofins Genomics). The GUS gene was designed as a fusion protein with the neomycin resistance gene (NeoR), connected via a C-terminal SGGGGS linker, and expressed as a single transcriptional unit. Although GUS alone can serve as a reporter for visual screening, its expression level may vary depending on the genomic integration site or due to transcriptional instability, which can result in weak staining and false-negative identification of transformants. To overcome these limitations and achieve more consistent and reliable blue staining of colonies, the GUS gene was fused with NeoR. Selection using NeoR ensures that only transformants with stable integration and active transcription of the fusion gene are recovered, thereby enhancing the reliability of GUS-based screening.

To construct the GUS-NeoR expression cassette, inverse PCR was performed using a thraustochytrid expression vector containing the NeoR expression cassette, comprising the *T. aureum*-derived ubiquitin promoter, NeoR gene, and SV40 terminator [31,32], as template DNA. The inverse PCR was carried out using Tks Gflex™ DNA Polymerase (Takara Bio Inc.) with primers Linker-NeoR-S and UbiP-A (Supplemental Table 1). Separately, the codon-optimized GUS gene was amplified using primers UbiP-GUS-S and Linker-GUS-A (Supplemental Table S1). The resulting GUS PCR product was inserted between the ubiquitin promoter and NeoR gene using the In-Fusion HD Cloning Kit (Takara Bio Inc.), generating the GUS-NeoR fusion construct. For genomic integration, the linearized construct was amplified using primers Transfection-S and Transfection-A (Supplemental Table S1). The construct was introduced into *A. limacinum* ATCC MYA-1381 via electroporation using a Gene Pulser Xcell (Bio-Rad Inc.) at 750 V, 25 μF, and 200 Ω in a 1 mm-gap electroporation cuvette (NEPA GENE Co. Ltd), following the protocol described in [33]. For *T. aureum* ATCC 34304, cells were cultured in GY medium at 25 °C for 3 days, and 1 mL of culture was spread onto PDA plates. Gold particles (0.6 μm diameter; Bio-Rad Inc.) were coated with 1.4 μg of the linearized GUS-NeoR construct and delivered using the PDS-1000/He Biolistic Particle Delivery System (Bio-Rad Inc.) equipped with a 1100 psi rupture disk, as described in [23]. After transfection, *A. limacinum* ATCC MYA-1381 and *T. aureum* ATCC 34304 were incubated overnight at 25 °C. Cells were spread onto PDA plates containing 0.5 mg/mL G418 for selection. To visualize blue-stained colonies, 100 μL of 10 mg/mL 5-bromo-4-chloro-3-indolyl-β-D-glucuronide (X-Gluc, Apollo Scientific Ltd) was evenly spread onto a 100-mm diameter PDA plate.

2.3. Preparation of RNP

The crRNA recognizing the target genes were designed using the online tool provided by Integrated DNA Technologies (IDT Inc.) (https://sg.idtdna.com/site/order/designtool/index/CRISPR_SEQUENCE). Three crRNAs were constructed for each gene, with each recognizing a different sequence. Two μL of 100 μM crRNA was mixed with 2 μL of 100 μM tracrRNA (IDT Inc.) and 16 μL of Nuclease Free Duplex Buffer (IDT Inc.). The solution was incubated at 95 °C for 5 min and then cooled at room temperature for 30 min to generate 10 μM guide RNA (gRNA). To prepare the gRNA mixture, 4 μL of each distinct gRNA was combined, resulting in a total volume of 12 μL. When a single type of gRNA was used, the 12 μL gRNA solution contained only that specific gRNA. The gRNA was then mixed with 2.4 μL of 62 μM Alt-R® S.p. Cas9 Nuclease V3 (IDT Inc.), and the final solution was brought to a volume of 16 μL by adding D-PBS. The solution was gently mixed by pipetting and incubated at room temperature for 30 min to form an RNP complex.

2.4. Transfection of RNP

2.4.1. Preparation of A. limacinum ATCC MYA-1381 and T. aureum ATCC 34304 for RNP transfection

The GUS-expressing *A. limacinum* ATCC MYA-1381 and *T. aureum* ATCC 34304 were pre-cultured in 3 mL of GY medium at 25 °C shaking at 150 rpm for 3 days. The culture was then transferred into 3 mL of dGPY medium (0.2% glucose, 0.1% polypeptone, and 0.05% yeast extraction in 1.75% artificial sea water) to adjust the OD_{600} to 1.0. After 4 h of shaking culture in a test tube, cells were collected by centrifugation at 2000 ×*g* for 2 min and washed twice with 1.75 % artificial sea water and OPTI-MEM (Thermo Fisher Scientific Inc.). Cells were resuspended in 50 μL of OPTI-MEM, and 24 μL of cell suspension was mixed with 8 μL of RNP, then transferred to 1 mm electroporation cuvette.

2.4.2. Preparation of P. sarkarianum SEK364 for RNP transfection

P. sarkarianum SEK364 was cultured in 3 mL of GY medium at 25 °C with shaking at 150 rpm for 7 days. After incubation, the culture was harvested by centrifugation at 5000 ×*g* for 2 min. The volume of the collected culture was adjusted using the formula: initial culture volume (typically 3 mL) × ($1/OD_{600}$ of the 7-day culture sample). The supernatant was removed, then cells were washed twice with 300 μL of 1.75 % artificial sea water and 300 μL of OPTI-MEM. Cells were resuspended in 100 μL of OPTI-MEM, and 22 μL of cell suspension was mixed with 16 μL of RNP, then transferred to 1 mm electroporation cuvette.

2.4.3. Electroporation and recovery culture

Using the Gene Pulser Xcell system, cells were exposed to two consecutive exponential decay pulses with no interval, under conditions of 750 V/mm, 25 μF, 200 Ω, and a 1 mm gap distance. Immediately after pulsing, 800 μL of GY medium was added, and the cells were incubated overnight at 25 °C with rotary culture. Following the recovery culture, cell numbers were quantified using a hemocytometer. The samples were then diluted in 200 μL of GY medium to achieve approximately 100 colonies per one plate (100 mm diameter), then spread onto PDA plate. For GUS-expressing *A. limacinum* ATCC MYA-1381 and *T. aureum* ATCC 34304, the diluted sample was spread onto PDA supplemented with 100 μL of 10 mg/mL X-Gluc and cultivated at 25 °C.

2.5. Screening of genome-edited strains

To evaluate genome editing efficiency, colony formation and pigmentation development were monitored in GUS-expressing *A. limacinum* ATCC MYA-1381 and *T. aureum* ATCC 34304. *T. aureum* ATCC 34304 exhibited slower growth compared to *A. limacinum* ATCC MYA-1381, requiring a longer incubation period for colony formation and the development of blue pigmentation. Colonies of *A. limacinum* were assessed for pigmentation approximately 10 days after inoculation, whereas *T. aureum* colonies were evaluated after approximately 30 days under the same culture conditions. Colony color was used as an indicator of genome editing outcomes. Blue and white colonies were manually counted, and the ratio of white colonies was used to quantify genome editing efficiency. These white colonies were then isolated and cultured in 800 μL of GY medium by rotary culture for 2 days. Due to the inability to use color-based selection for genome editing of the *ELO/DES* genes in *P. sarkarianum* SEK364, colonies grown on PDA plates were randomly picked and inoculated into a deep-well 96-well plate (Thermo Scientific), with each well containing 600 μL of GY medium. A breathable plate seal (BM Equipment) was applied to allow gas exchange, and the plate was incubated at 25 °C with shaking at 135 rpm by using MaxMixer EVR-034 (TAITEC) for 2 days. Five μL of the culture medium was mixed with 45 μL of a 22 mM NaOH solution and incubated at 37 °C for 10 min to extract genomic DNA. PCR was performed using the extracted DNA as

a template and the primer set described in Supplemental Table S1. Following electrophoresis, the PCR product was excised from the gel, purified, and subjected to sequencing analysis service (Azenta life sciences) to verify the success of the genome editing. The waveform data figures with quality value (QV) and schematic diagram of gene expressing construct were created using SnapGene Viewer (version 7.2.1).

2.6. Gas chromatography (GC) analysis to determine the fatty acid composition of WT and genome-edited strains of P. sarkarianum SEK364

Cells were cultured in a 50 mL flask containing 20 mL of GY medium at 25 °C or 18 °C with shaking at 150 rpm. One mL of culture fluid was harvested, and cells were collected by centrifugation (2500 ×*g*, 3 min), dried by lyophilization, and their DCW was measured. The fatty acids were extracted as fatty acid methyl esters (FAMEs) from dried cells as described in [34]. Briefly, dried cells were incubated overnight at 45 °C with 0.2 mL toluene, 1.5 mL methanol, 0.3 mL 8 % methanolic-HCl, and 50 μL of 10 mg/mL lauric acid (as an internal standard) to prepare FAMEs. The resulting mixture was then combined with 1 mL of hexane and 1 mL of water, followed by centrifugation at 600 ×*g* for 3 min. The upper hexane layer was transferred to a new tube. FAMEs were analyzed by GC using a GC-2014 system (Shimadzu) equipped with an ULBON HR-SS-10 column (Shinwa Chemical Industries) and a flame ionization detector. The column temperature was programmed to increase from 160 °C to 200 °C by 2 °C/min, and then from 200 °C to 220 °C by 5 °C/min. The molecular species of fatty acids were identified by comparing with the retention time of each standard. Especially, cis-4,10,13,16-docosatetraenoic acid, which was used as standard for a non-methylene-interrupted (NMI) fatty acid, was purchased from Cayman chemical.

2.7. Determination of the unsaturated bonds of NMI-DPA by liquid chromatography-electrospray ionization tandem mass spectrometry (LC-ESI MS/MS) after epoxidation

Cells were collected by centrifugation (5000 ×*g*, 3 min), then the cell pellet was resuspended in 250 μL distilled water, then crushed at 3000 rpm for 60 s using a μT-12 bead beater (TAITEC) with glass beads (diameter: 0.6 mm, AS ONE), and kept on ice for 60 s. This procedure was repeated three times to prepare the cell lysate. Cellular lipids were extracted from 50 μL of cell lysate by adding 200 μL of chloroform/methanol (2:1, *v*/v). After incubation at 37 °C for 30 min with shaking at 2000 rpm using ThermoMixer C (Eppendorf), the mixture was centrifuged at 11,000 ×*g* for 3 min. The lipid fraction extracted from Δ5DES KO strain was treated with 0.2 M KOH at 37 °C for 16 h for alkaline hydrolysis to release fatty acids from phospholipids and neutral lipids. After the reaction, the mixture was neutralized by adding an appropriate amount of acetic acid, followed by a two-phase separation using the Bligh and Dyer method [35]. For the epoxidation, 10 μL of the lower phase containing fatty acids was mixed with 10 μL of 20 mM meta-chloroperoxybenzoic acid (mCPBA), which is dissolved in acetonitrile/isopropyl alcohol/water = 65/30/8, *v*/v/v, and reacted at 50 °C for 80 min [36]. mCPBA was obtained from Tokyo Chemical Industry Co., LTD. As a negative control, same fraction was processed under the same conditions without mCPBA. The reaction product was then dissolved in 150 μL of acetonitrile/isopropyl alcohol/water (65/30/8, v/v/v) and centrifuged at 20,000 ×*g* for 5 min. Subsequently, 120 μL of the supernatant was transferred to an autoinjector vial. MS/MS analysis was performed on the precursor ion *m/z* 345, corresponding to epoxidized NMI-DPA, using a collision energy (CE) of −25 to induce collision-induced dissociation (CID) using LC-ESI MS/MS (3200 QTRAP, SCIEX, MA, USA), thereby generating diagnostic fragment ions characteristic of epoxidized unsaturated bonds. A binary solvent gradient with a 200 μL/min flow rate was used to separate free fatty acid by reverse-phase chromatography using an InertSustain C18 column (2.1 × 150 mm, 5 μm, GL Sciences, Japan) as described in [23].

2.8. Targeted lipidomics by LC-ESI MS/MS

Cells were collected by centrifugation (5000 ×*g*, 3 min), then the cell pellet was resuspended in 250 μL distilled water, then crushed at 3000 rpm for 60 s using a μT-12 bead beater (TAITEC) with glass beads (diameter: 0.6 mm, AS ONE), and kept on ice for 60 s. This procedure was repeated three times to prepare the cell lysate. Cellular lipids were extracted from 50 μL of cell lysate by adding 200 μL of chloroform/methanol (2:1, *v*/v). After incubation at 37 °C for 30 min with shaking at 2000 rpm using ThermoMixer C (Eppendorf), the mixture was centrifuged at 11,000 ×*g* for 3 min. Fifty microliters of the organic phase were transferred to autoinjector vials containing 550 μL of 2-propanol, and then the cellular lipids were measured using LC-ESI MS/MS (3200 QTRAP, SCIEX, MA, USA) in multiple reaction monitoring (MRM) mode. A binary solvent gradient with a 200 μL/min flow rate was used to separate phospholipids and neutral lipids by reverse-phase chromatography using an InertSustain C18 column (2.1 × 150 mm, 5 μm, GL Sciences, Japan) as described in [37]. For phosphatidylcholine (PC), the fragment ion at *m/z* 184 derived from the phosphocholine head group was used as the product ion (Q3), whereas for triacylglycerol (TG), the neutral loss corresponding to one fatty acid moiety was selected as Q3 [37,38]. Precursor ions (Q1) were constructed based on the molecular masses of PC and TG species containing the following fatty acids: C14:0, C16:0, C18:0, C18:1, C18:2, C18:3, C20:3, C20:4, C20:5, C22:4, C22:5, and C22:6. MRM conditions for the quantification of individual molecular species of PC and TG were as described previously [23]. Chromatographic peaks were analyzed using MultiQuant software (version 3.0.1, SCIEX). Lipidomics data were processed for heatmap visualization using ClustVis [39]. Transformation was performed by applying the natural logarithm [ln(x)], followed by row-wise normalization through unit variance scaling. TG species composed exclusively of C16:0, C18:0, and C18:1 were excluded from the heatmap analysis, thereby restricting the dataset to TGs incorporating at least one LC-PUFA.

2.9. Evaluation of substrate specificity of C20ELO using Saccharomyces cerevisiae

To evaluate the substrate specificity of C20ELO, *S. cerevisiae* transformants harboring either a C20ELO-expressing vector or a mock vector were first cultured in synthetic complete (SC)-ura medium containing 2 % glucose at 25 °C for 1 day, followed by an additional 1 day in SC-ura medium supplemented with 2 % galactose and 50 μM DGLA (C20:3) or ARA (C20:4n-6), as described previously [23]. Cells were harvested by centrifugation at 5000 ×*g* for 3 min, resuspended in 200 μL of distilled water, and disrupted using a bead beater (μT-12, TAITEC) with 0.4 mm glass beads (AS ONE Corp.) at 3000 rpm for 60 s, followed by cooling on ice for 60 s. This cycle was repeated three times to prepare cell lysates. Lipids were extracted from 90 μL of lysate by adding 375 μL of chloroform/methanol (1:2, *v*/v). For saponification, 10 μL of 4 M KOH was added, and samples were incubated at 37 °C for 3 h. Subsequently, 10 μL of 2 M acetic acid, 125 μL of chloroform, and 125 μL of water were added, and the organic phase was separated by centrifugation at 17,500 ×*g* for 3 min. C20:3 (*m/z* 305), C20:4 (*m/z* 303), C22:3 (*m/z* 333), and C22:4 (*m/z* 331) were quantified by negative-ion mode MRM as described previously [23]. In addition, FAMEs were prepared from the organic phase, and peaks corresponding to C20:3, C20:4, C22:3, and C22:4 were detected by GC. C20ELO activity was calculated using the following formula: activity (%) = product area × 100 / (substrate area + product area).

2.10. Microscopic observation of WT and genome-edited strains of P. sarkarianum SEK364

Lipid droplets (LDs) were stained using HCS LipidTOX™ Red Neutral

Lipid Stain (Thermo Fisher Scientific) and observed under a DMi8 fluorescence microscope equipped with a Texas Red filter set (excitation: 540–580 nm; dichroic mirror: 585 nm; emission: 592–668 nm), a DFC3000G camera, and Leica Application Suite X (LAS X) software. Imaging was performed using a 100× oil immersion objective lens (numerical aperture 1.40).

2.11. Quantitative real-time PCR (qPCR)

Total RNA was extracted from WT and genome-edited strains of *P. sarkarianum* SEK364 after 4 days of culture at 25 °C using Sepasol-RNA I Super G (Nacalai Tesque), then purified through ReliaPrep™ RNA Miniprep Systems (Promega). cDNA was synthesized from 1 μg of total RNA using the PrimeScript™ RT reagent Kit with gDNA Eraser (Perfect Real Time; Takara Bio Inc.), following the manufacturer's instructions. qPCR was performed using an Mx3000P qPCR System (Agilent Technologies) with SYBR™ Green qPCR Master Mix (thermo scientific) by using cDNA as a template. mRNA expression levels of genes involved in the ELO/DES pathway were quantified using the ΔΔCt method, incorporating PCR amplification efficiencies for each target gene [40]. The following genes were selected as targets: *C16ELO* (accession no. LC530191), *C18ELO* (LC530192), *C20ELO* (LC530193), *Δ9DES* (LC530194), *Δ12DES* (LC530195), *Δ6DES* (LC530196), *Δ5DES* (LC530197), *Δ4DES* (LC530198), and *ω3DES* (LC530199). Three housekeeping genes, elongation factor 1α (EF1α), β-tubulin, and β-actin, were used as reference genes for normalization. Using amino acid sequences of *S. cerevisiae* genes as queries, we retrieved the corresponding housekeeping genes from the draft genome of *P. sarkarianum* (accession numbers BLSF01000001 to BLSF01000360). The suitability of EF1α, β-tubulin, and β-actin was evaluated by sequence similarity analysis using NCBI BLAST. Oligonucleotide primer sets for qPCR are shown in Supplemental Table S1.

2.12. Statistical analysis

Statistical analyses were performed using GraphPad Prism version 6.05 for Windows (GraphPad Software). Two-group comparisons were analyzed using an unpaired, two-tailed Student's *t*-test. For comparisons among multiple groups, one-way ANOVA was conducted, followed by Tukey's test for all pairwise comparisons or Dunnett's test when comparing each group to the WT control. Quantitative data are presented as mean ± standard deviation (SD). Statistical significance is indicated as follows: $p < 0.05$; **, $p < 0.01$; ***, $p < 0.001$.

3. Results

3.1. Assessment of the feasibility of transgene-free, protein-based genome editing using GUS-expressing, color-selectable Aurantiochytrium limacinum ATCC MYA-1381 and Thraustochytrium aureum ATCC 34304

To date, transgene-free, RNP-mediated genome editing has not been reported in thraustochytrids, highlighting the need to establish protocols for efficient RNP delivery into these organisms. *A. limacinum* ATCC MYA-1381, also known *as Schizochytrium limacinum* SR21 and recognized for its rapid growth among thraustochytrids [41], was selected as a model organism to enable iterative optimization through increased experimental frequency. For visual assessment of gene expression, we employed the β-glucuronidase (GUS) reporter system, which catalyzes the hydrolysis of chromogenic substrates such as X-Gluc (5-bromo-4-chloro-3-indolyl-β-D-glucuronide), yielding a distinct blue precipitate upon enzymatic cleavage. In this study, we generated GUS-expressing *A. limacinum* by the transfection of *GUS-NeoR* fused gene construct conferring color selection and G418 resistance (Fig. 1A). The GUS-expressing strain was subjected to electroporation with an RNP complex consisting of crRNA targeting the *GUS* gene, tracrRNA, and Cas9. Initially, the potential for modifying the *GUS* gene was assessed using crRNA1, which targets the protospacer adjacent motif (PAM) sequence located 130 base pairs downstream of the start codon (Fig. 1A). As a result, not only blue colonies but also white colonies were observed on the PDA plate supplemented with X-Gluc, indicating successful disruption of the *GUS* gene by the transfection of RNP (Fig. 1B). The sequence analysis revealed various patterns of insertion and deletion (indel) mutations originating from the cleavage site corresponding to the designed crRNA1 sequence (Fig. 1C). Genome editing efficiency was estimated based on the frequency of white colonies, yielding a maximum of 27 % (Fig. 1D). Across 10 experiments, the average genome editing efficiency was 7.5 %. To evaluate whether genome editing using RNP is feasible in phylogenetically distinct genera of thraustochytrids, we investigated the applicability of this method to GUS-expressing *T. aureum* ATC34304. Consistent with *A. limacinum* ATCC MYA-1381, the introduction of RNP led to the formation of white colonies, indicating successful disruption of the *GUS* gene of *T. aureum* ATCC 34304 (Fig. 1E). Sequence analysis of the *GUS* gene confirmed that mutations were introduced precisely at the target site defined by the designed crRNA1 (Supplemental Fig. 1A). Because *T. aureum* ATCC 34304 is essentially diploid [42], sequencing chromatograms displayed overlapping peaks and reduced quality value originating from the cleavage site, indicating of heterozygous indel mutations [43]. Based on the number of white colonies, genome editing efficiency was calculated across three independent trials. The maximum genome editing efficiency observed was maximum of 24 % with some variability across experiments (Fig. 1D). These results indicated that the RNP delivery condition that we developed is not limited to a specific genus.

Based on these findings, we employed transgene-free, RNP-based genome editing to modify the ELO/DES pathway in *P. sarkarianum* SEK364. Selecting genome-edited *P. sarkarianum* strains was challenging because no selectable marker or obvious phenotypic change was available. Unlike systems that use antibiotic resistance or visible traits from gene disruption, our method provided no such selective pressure. As a result, edited strains could only be identified through molecular screening, making the process difficult and time-consuming. Moreover, our results revealed that the efficiency of RNP-mediated genome editing in thraustochytrids was not consistently high (Fig. 1D). Therefore, we estimated that screening hundreds of colonies would be necessary to isolate genome-edited strains of *P. sarkarianum* SEK364. To detect indel mutations using a single crRNA, the heteroduplex mobility assay (HMA), which requires polyacrylamide gel electrophoresis (PAGE), and the T7 endonuclease I digestion assay are commonly employed [44]. However, due to the time-consuming steps involved, such as heteroduplex formation, PAGE gel preparation, and the high cost of endonucleases, these methods are impractical for large-scale screening. Therefore, we explored the use of at least two crRNAs to induce extensive deletions in the target gene via multiple cleavage events, yielding smaller PCR products that can be readily detected using standard agarose gel electrophoresis. RNP complexes containing two crRNAs, crRNA2 and 3, targeting distant regions in the *GUS* gene, were introduced into GUS-expressing *A. limacinum* ATCC MYA-1381 (Fig. 1A). As expected, PCR products with substantially reduced size were detected in two out of four white colonies generated by transfection with RNPs containing both crRNA2 and crRNA3 (Fig. 1F). Sequencing analysis of the PCR products confirmed that crRNA-dependent dual-site cleavage occurred in white colony No. 2 (Fig. 1F and Supplemental Fig. 1B, C). On the other hand, no cleavage by crRNA2 was detected in white colony No. 1, where the PCR product size was almost identical to that of the control (Fig. 1F). Mutations exclusively induced by crRNA3 were detected in white colony No. 1 specifically affecting the N—K motif, which is critical for GUS activity [45] (Supplemental Fig. 1D). These results indicated that the use of two distinct crRNAs enables not only single-site cleavage but also dual-site cleavage. We attempted to establish genome-edited strains of *P. sarkarianum* SEK364 targeting the ELO/DES pathway by employing a screening strategy based on the reduction in PCR product size resulting from dual-site cleavage.

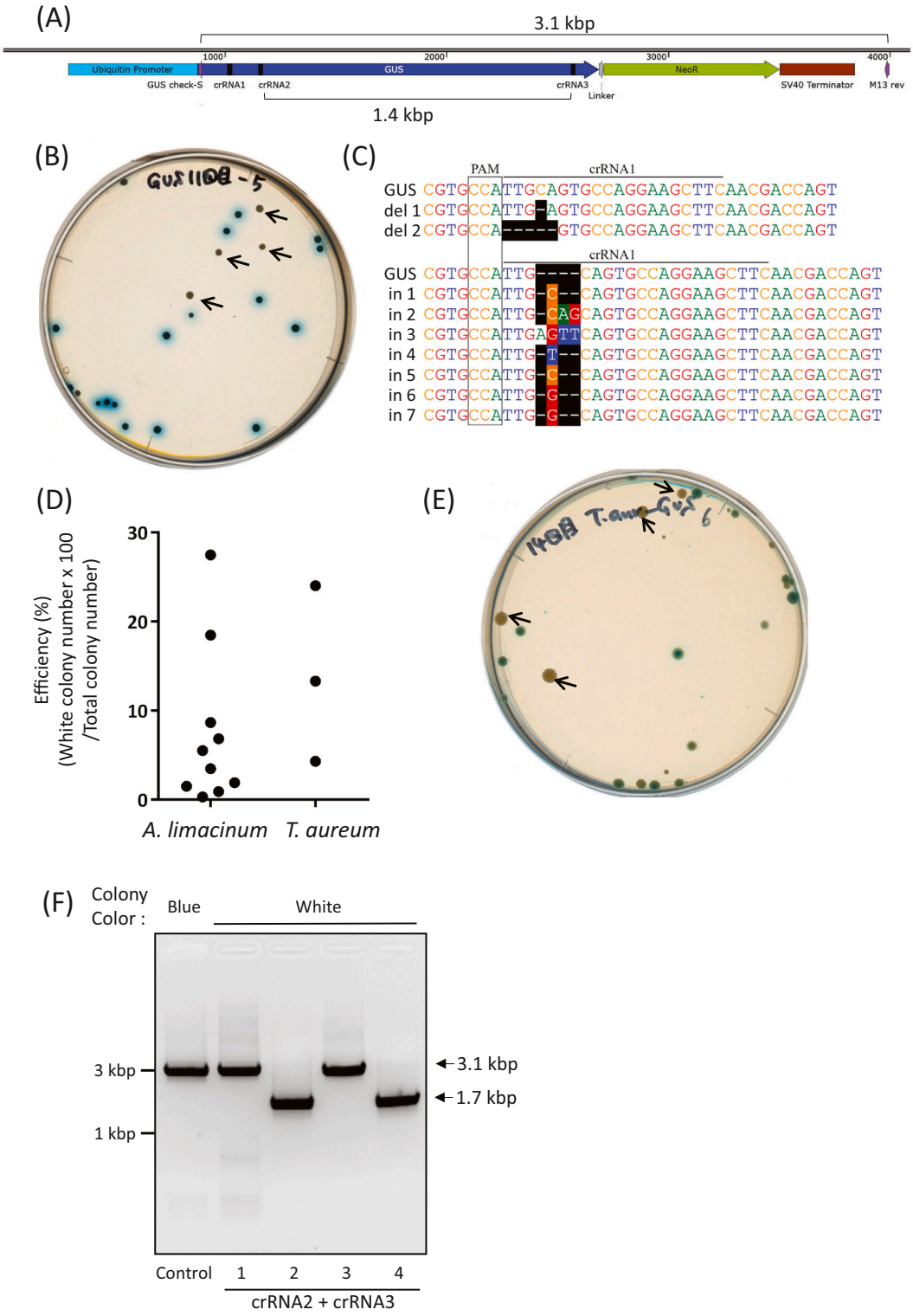

Fig. 1. RNP-mediated genome editing of GUS-expressing *Aurantiochytrium limacinum* ATCC MYA-1381 and *Thraustochytrium aureum* ATCC 34304
(A) Schematic diagram of the crRNA target sites in *GUS* gene. (B) Representative picture of X-Gluc-mediated blue-white selection of *A. limacinum* ATCC MYA-1381 after the introduction of crRNA1 containing RNP. Four colonies on the plate did not exhibit blue coloration. (C) Sequence analysis of PCR products of white colonies of *A. limacinum* ATCC MYA-1381. Deletions (del 1, 2) of 1 or 5 bases, as well as insertions (in 1–7) of 1 to 4 bases, were observed upstream of the PAM sequence. (D) Genome editing efficiency based on blue-white selection. Genome editing efficiency (%) was calculated as follows: white colony number ×100/total colony number. Genome editing efficiency of *A. limacinum* ATCC MYA-1381 *and T. aureum* ATCC 34304 was calculated from ten and three independent experiments, respectively. (E) Representative picture of X-Gluc-mediated blue-white selection of *T. aureum* ATCC 34304 after the introduction of RNP. (F) PCR-based confirmation of dual-site cleavage using two crRNAs targeting distinct sequences within the *GUS* gene. As illustrated in (A), successful excision at both target sites results in a PCR product lacking a 1.4 kbp. Among the four white colonies obtained, two exhibited simultaneous cleavage at two target sites in this experiment.

3.2. Application of transgene-free, protein-based genome editing for *P. sarkarianum* SEK364

In this study, we performed genome editing on three targets (two desaturates and one elongase), which are enzymes involved in the DHA synthesis of *P. sarkarianum* SEK364, as illustrated in Fig. 2A. The first target, Δ4 desaturase (Δ4DES), acts on docosatetraenoic acid (DTA, C22:4n-6) and n-3DPA, converting them to n-6 docosapentaenoic acid (n-6DPA, C22:5n-6) and DHA, respectively (Fig. 2A). By disrupting the gene encoding Δ4DES, the conversion to DHA is blocked, making DTA and n-3DPA the major LC-PUFA in the genome-edited strain. Our second target, C20 elongase (C20ELO), elongates carbon chains from C20 to C22, converting ARA and EPA into DTA and n-3DPA, respectively (Fig. 2A). Therefore, knocking out C20ELO could yield strains that produce the beneficial fatty acids ARA and EPA at high levels. In a previous study, Δ4DES and C20ELO knockout (KO) strains were generated by disrupting the target genes using heterologous antibiotic resistance markers for selection [23]. The desired LC-PUFAs were successfully accumulated in the KO strains without any impairment of growth, indicating that deletion of these genes is non-lethal. Therefore, these target genes represent ideal candidates for genome editing evaluation. In addition to these two genes, we knock out the Δ5 desaturase (Δ5DES) gene by genome editing in this study. Δ5DES acts on DGLA and ETA, converting them to ARA and EPA, respectively (Fig. 2A). By disrupting Δ5DES, this pathway could be blocked to generate a genome-edited strain that accumulates DGLA and ETA.

For the Δ4DES KO strain, 280 colonies were screened to obtain genome-edited strains based on changes in PCR product size caused by

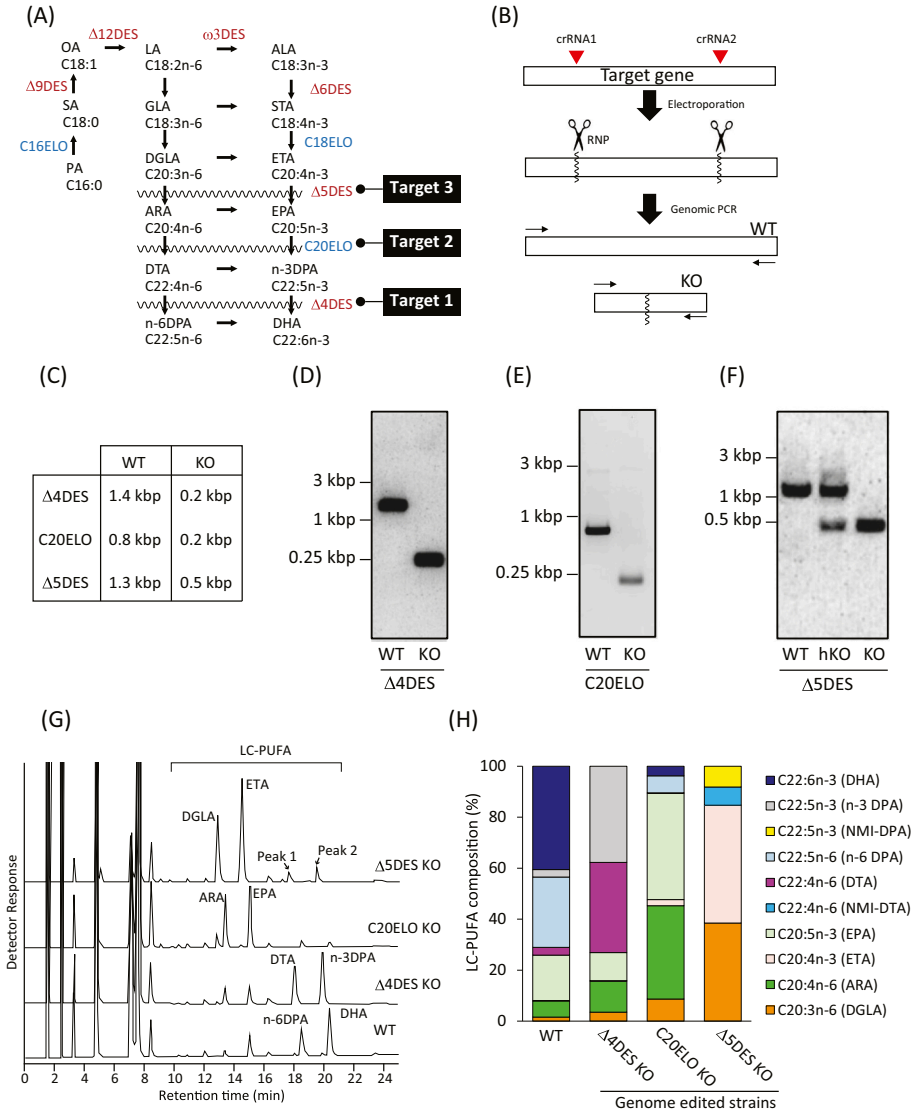

Fig. 2. Target genes and generation of genome-edited strains of *Parietichytrium sarkarianum* SEK364
(A) DHA biosynthetic pathway in *P. sarkarianum* SEK364. The sequential action of elongases (ELOs) and desaturases (DESs) facilitates the synthesis of DHA or n-6DPA via intermediate metabolites with varying carbon chain lengths and degrees of unsaturation. In this study, three enzymes, Δ4DES (Target 1), C20ELO (Target 2), and Δ5DES (Target 3), were selected as targets for genome editing. (B) Screening strategy for genome-edited strains. Two distant cleavage sites were selected within the target gene, and genome-edited strains were identified based on a marked reduction in PCR product size, as summarized in (C). PCR analysis of target genes in WT and genome-edited strains: (D) Δ4DES KO, (E) C20ELO KO, and (F) Δ5DES KO. Genome-edited strains exhibited PCR products of different sizes compared to the WT, confirming successful genome editing. The Δ5DES heterozygous knockout (hKO) strain was initially generated by introducing an RNP complex targeting Δ5DES into the WT. A second round of RNP delivery was subsequently performed on the Δ5DES hKO strain to obtain the Δ5DES homozygous KO strain. (G) GC chromatograms of FAMEs from WT and genome-edited strains. Fatty acid species were identified by comparing retention times with those of authentic standards. Peak1 and peak2 that did not match any standards in the Δ5DES KO strain are indicated by arrows on its chromatogram. (H) LC-PUFA composition in WT and genome-edited strains.

dual-site DNA cleavage at the target sites of crRNA (Fig. 2B, C). Among them, four strains exhibited PCR products of the expected size. The results for one representative strain are shown in Fig. 2D. Sequence analysis of PCR products derived from both the wild type (WT) and Δ4DES KO strains confirmed that cleavage occurred at the crRNA target sites (Supplemental Fig. 2A, B). Next, one C20ELO KO strain with PCR product corresponding to dual-site cleavage was obtained by screening of 196 colonies (Fig. 2C, E). Sequencing of PCR product of C20EKO KO strain validated the occurrence of cleavage at both designed crRNA target sites (Supplemental Fig. 2C, D). Based on previous observations, *P. sarkarianum* SEK364 is presumed to be predominantly diploid [23]. Nevertheless, we found that both alleles of the target genes could be simultaneously cleaved by RNP introduction, enabling the generation of Δ4DES and C20ELO KO strains in a single step (Fig. 2D, E). In contrast, no strains exhibiting dual-site cleavage of both alleles were obtained following a single introduction of the RNP complex targeting the *Δ5DES* gene. Alternatively, a Δ5DES heterozygous KO (hKO) strain was obtained during the initial screening of 528 colonies (Fig. 2F). To generate the homozygous Δ5DES KO strain, the hKO strain was applied for a second RNP introduction. This approach resulted in the generation of Δ5DES KO showing only a short PCR product from a subsequent screening of 288 colonies (Fig. 2C, F). Sequence analysis of the PCR product of Δ5DES KO strain confirmed dual-site cleavage at the crRNA-targeted sites (Supplemental Fig. 2E, F). These findings demonstrate that the RNP-based genome editing method, which avoids the introduction of transgenes, enables the successful generation of strains with desired modifications in the LC-PUFA metabolic pathway of *P. sarkarianum* SEK364.

3.3. Fatty acid compositions of WT and genome-edited strains

Next, we investigated the impact of genome editing on the composition of LC-PUFAs. GC analysis revealed that chromatograms of FAMEs were remarkably altered in genome-edited strains compared to WT (Fig. 2G). The peaks corresponding to n-6DPA (C22:5n-6) and DHA (C22:6n-3), which were predominant in WT, completely disappeared in Δ4DES KO strain (Fig. 2G). Consequently, peaks corresponding to DTA (C22:4n-6) and n-3DPA (C22:5n-3) were detected in the Δ4DES KO strain (Fig. 2G). The LC-PUFA composition of the WT and Δ4DES KO strains showed marked differences. Specifically, while DTA (C22:4n-6) and n-3DPA (C22:5n-3) were scarcely detected in WT, the Δ4DES KO strain showed the capacity for their efficient production, indicating that the successful establishment of a highly DTA/n-3DPA productive strain (Fig. 2H). Similarly, C20ELO KO strain showed a drastically decrease of LC-PUFAs with chain lengths of 22 carbons, while ARA (C20:4n-6) and EPA (C20:5n-3) were enriched (Fig. 2G, H). For the Δ5DES KO strain, DGLA (C20:3n-6) and ETA (C20:4n-3), which were almost undetectable in WT, emerged as the primary LC-PUFAs (Fig. 2G, H). These findings demonstrate that genome editing can be effectively employed to the desirable production of LC-PUFAs by *P. sarkarianum* SEK364. Although the levels of DHA and n-6DPA were markedly reduced, they remained in the C20ELO KO strain (Fig. 2H). This residual synthesis is likely due to partial functional redundancy provided by other elongases that compensated for the loss of C20ELO [23].

3.4. Lipidomic profiling of WT and genome-edited strains of *P. sarkarianum SEK364*

To gain deeper insights into the lipid composition of WT and genome-edited strains, we performed targeted lipidomics focusing on phosphatidylcholine (PC) and triacylglycerol (TG) species composed of fatty acids ranging from C16:0 to C22:6. The analysis revealed distinct PC and TG profiles among WT and the various genome-edited strains (Supplementary Figs. 3 and 4). In WT cells, major PC species included PC38:6 and PC44:12, both containing DHA (C22:6), as well as lysophosphatidylcholine (LPC) 22:6. In contrast, Δ4DES KO and Δ5DES KO strains exhibited markedly reduced levels of these DHA-containing PCs and LPCs (Supplementary Fig. 3). Notably, the C20ELO KO strain showed increased levels of PC40:9, PC40:10, PC34:5, and PC36:5, which are presumed to contain ARA (C20:4) or EPA (C20:5). In Δ4DES KO cells, PC species such as PC42:9, PC38:4, PC44:8, and LPC22:4 were elevated, indicating the accumulation of DTA (C22:4). Additionally, PC44:9 and LPC22:5, which contain n-3DPA (C22:5n-3), were also detected. In Δ5DES KO strains, LPC20:3, LPC20:4, PC34:3, PC36:3, PC40:7, and PC40:8 were elevated, suggesting the incorporation of DGLA (C20:3) and ETA (C20:4n-3).

We next examined TG species, which serve as key storage lipids for LC-PUFAs. TGs composed solely of palmitic acid (C16:0), stearic acid (C18:0), and oleic acid (C18:1) were excluded from the analysis to focus on TGs containing at least one LC-PUFA. In WT cells, TGs predominantly incorporated DHA (C22:6), whereas in Δ4DES KO strains, TGs containing DTA (C22:4) and n-3DPA (C22:5n-3) were the major species (Supplementary Fig. 4). In C20ELO KO strains, TGs containing EPA (C20:5) and ARA (C20:4) were enriched, while Δ5DES KO strains primarily synthesized TGs containing DGLA (C20:3) and ETA (C20:4n-3). Collectively, these lipidomic analyses demonstrate that genome-edited strains produce the expected LC-PUFAs in accordance with the targeted gene disruptions, and that the synthesized LC-PUFAs are effectively incorporated into both PC and TG biosynthetic pathways.

3.5. Identification of newly synthesized fatty acid in *Δ5DES KO strain*

During GC analysis of fatty acid composition, two unknown peaks (designated as Peak 1 and Peak 2) were detected in the Δ5DES knockout (KO) strain. These peaks did not correspond to the retention times of commonly used standards (Fig. 2G). Additionally, lipidomic analysis identified PC species such as PC44:8, PC44:9, and PC44:10 in the Δ5DES KO strain, which are indicative of the incorporation of C22:4 and C22:5 LC-PUFAs (Supplementary Fig. 3). In general, adjacent double bonds in LC-PUFAs are separated by a methylene group. In mammals, FADS2 is known to function as a Δ6DES, and its genetical deletion results in a metabolic bypass where elongase and Δ5DES (FADS1) act without forming the Δ6DES-derived unsaturated bond. This bypass leads to the synthesis of non-methylene-interrupted (NMI) -PUFA, sciadonic acid (C20:3n-6, cis-5,11,14-eicosatrienoic acid), as previously reported [46]. We hypothesized that the unknown fatty acids detected in the Δ5DES KO strain were NMI-PUFAs generated through metabolic processing that skipped Δ5 desaturation (Supplemental Fig. 5). To test this hypothesis, we compared the chromatogram of the unknown fatty acid with commercially available NMI-PUFA, cis-4,10,13,16-docosatetraenoic acid (NMI-DTA) as a standard. The retention time of peak1 was identical to that of NMI-DTA, indicating that NMI-DTA was synthesized in the Δ5DES KO strain via the activity of C20ELO and Δ4DES in the absence of Δ5 desaturation (Fig. 3A and Supplemental Fig. 5). This result suggested that the peak2 detected in the Δ5DES KO strain would be cis-4,10,13,16,19-dcosapentaenoic acid (NMI-DPA) (Fig. 3A, Supplemental Fig. 5). To confirm the synthesis of NMI-DPA in the Δ5DES KO strain, we employed mCPBA epoxidation for lipid double-bond identification (MELDI) [36]. This method enables the epoxidation of unsaturated bonds in LC-PUFAs, allowing the detection of fragment ions corresponding to the positions of unsaturated bonds (Fig. 3B), thereby facilitating the structural determination of NMI-PUFAs. LC-PUFAs extracted from the Δ5DES KO strain were subjected to epoxidation, and multiple fragment ions were detected when reacted with mCPBA (Fig. 3C). In MELDI, dehydration product ion $[M\text{-}H\text{-}H_2O]^-$ is generated from epoxidized fatty acids by CID in negative ion mode [36]. The precursor ion of epoxidized NMI-DPA is $[M\text{-}H]^- = m/z$ 345, and its dehydration product ion $[M\text{-}H\text{-}H_2O]^-$ is m/z 327, which was detected in Fig. 3C, indicating successful epoxidation of NMI-DPA by mCPBA. The diagnostic fragment ions, such as m/z 183, 207, 223, 247, 263, and 287, demonstrated that the newly synthesized fatty acid in the Δ5DES KO is NMI-DPA (Fig. 3B, C). These results revealed that both n-6 and n-3 series

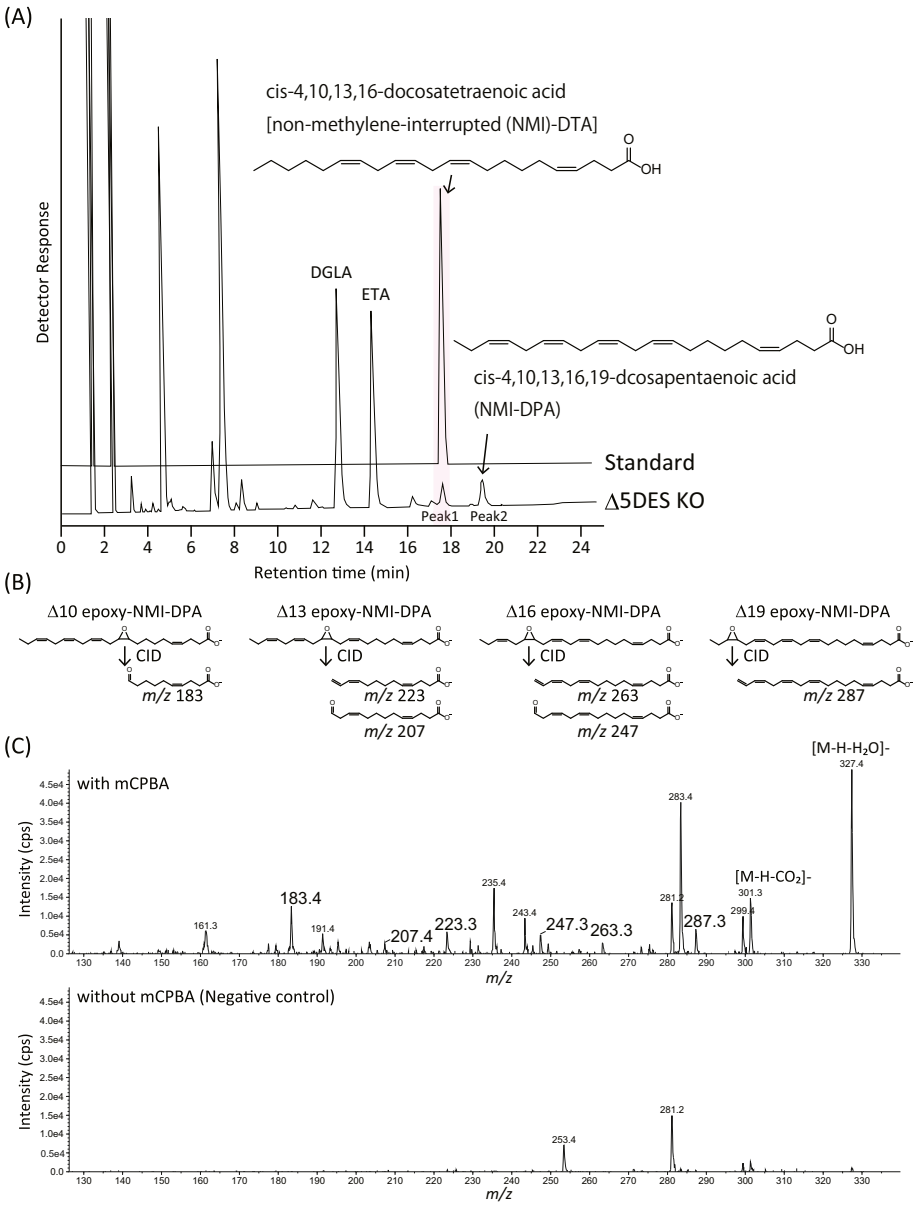

Fig. 3. Structural analysis of unknown LC-PUFAs generated in the Δ5DES KO strain.
(A) GC chromatograms of non-methylene-interrupted (NMI)-DTA (standard) and FAMEs of Δ5DES KO strain. The peak1 in the Δ5DES KO strain exhibited the retention time identical to NMI-DTA standard. (B) Fragmentation pattern of Δ10, Δ13, Δ16 and Δ19 -eploxy-NMI-DPA. To identify the structure of peak2, mCPBA epoxidation for lipid double-bond identification (MELDI) was applied to the lipid fraction extracted from Δ5DES KO strain. (C) MS/MS spectrum of lipid fraction extracted from Δ5DES KO strain with or without mCPBA. Fragment ions corresponding to the positions of unsaturated bonds in NMI-DPA were detected in mCPBA-reacted sample.

NMI-PUFAs are synthesized in the Δ5DES KO strain (Supplemental Fig. 5).

3.6. Substrate specificity of C20ELO of P. sarkarianum

To investigate whether C20ELO utilizes DGLA as a substrate and whether desaturation by Δ5DES affects its catalytic efficiency, we assessed elongase activity using C20ELO-expressing yeast, as established in our previous study [23]. At the time of galactose-induced expression, ARA (C20:4) and DGLA (C20:3) were supplemented, and their conversion to DTA (C22:4) and docosatrienoic acid (DTriA, C22:3), respectively, was examined. In mock controls, only unconverted ARA and DGLA were detected (Supplementary Fig. 6A, B), whereas C20ELO-expressing yeast synthesized C22:4 and C22:3, indicating elongation by two carbons and an increase of 28 in mass (Supplementary Fig. 6C, D). These results demonstrate that C20ELO can utilize DGLA as a substrate even without Δ5-desaturation and contribute to NMI-PUFA biosynthesis. Furthermore, methyl esters prepared from these samples were analyzed by GC to quantify substrate specificity based on peak areas corresponding to ARA, DGLA, DTA, and DTriA (Supplementary Fig. 6E). C20ELO exhibited elongation activity toward DGLA; however, ARA served as a more favorable substrate (Supplementary Fig. 6E), indicating that C20ELO recognizes Δ5-desaturation and that this feature influences its catalytic efficiency.

3.7. Evaluation of lipid droplet formation and growth capacity in WT and genome-edited P. sarkarianum SEK364 strains

Lipid composition analysis revealed that each genome-edited strain exhibited substantial alterations in LC-PUFA profiles and in the

molecular species of PC and TG, corresponding to the targeted disruption of metabolic enzymes in the ELO/DES pathway (Fig. 2A, Supplemental Figs. 3 and 4). We next evaluated how these alterations influence lipid droplet (LD) formation, which is associated with the accumulation of LC-PUFA, as well as the growth capacity of the strains. LDs were visualized by staining neutral lipids with LipidTOX and observing WT and genome-edited strains under a fluorescence microscope. We found that all strains displayed well-developed LDs (Fig. 4A), indicating that the genome-edited strains possess LD formation and lipid accumulation capacities comparable to those of the WT. To further examine the impact of genome editing on cell growth, biomass (dry cell weight, DCW) was measured between days 4 and 6 of cultivation at 25 °C. The genome-edited strains exhibited DCW slightly lower than WT but remained within a comparable range (Fig. 4B), indicating that they provide suitable platforms for producing target LC-PUFAs without apparent growth defects while maintaining lipid accumulation within LD.

3.8. Stability of LC-PUFA composition and productivity in genome-edited strains of P. sarkarianum SEK364

To evaluate the stability of genome-edited strains targeting metabolic enzymes in the ELO/DES pathway, we examined the impact of multiple passages on LC-PUFA composition and productivity. The results showed that, even after four consecutive passages, the genome-edited strains retained the LC-PUFA profiles (Fig. 5A). Strains established through transgene-free genome editing consistently maintained these properties, demonstrating the robustness and utility of the method developed in this study. Furthermore, analysis of total LC-PUFA levels

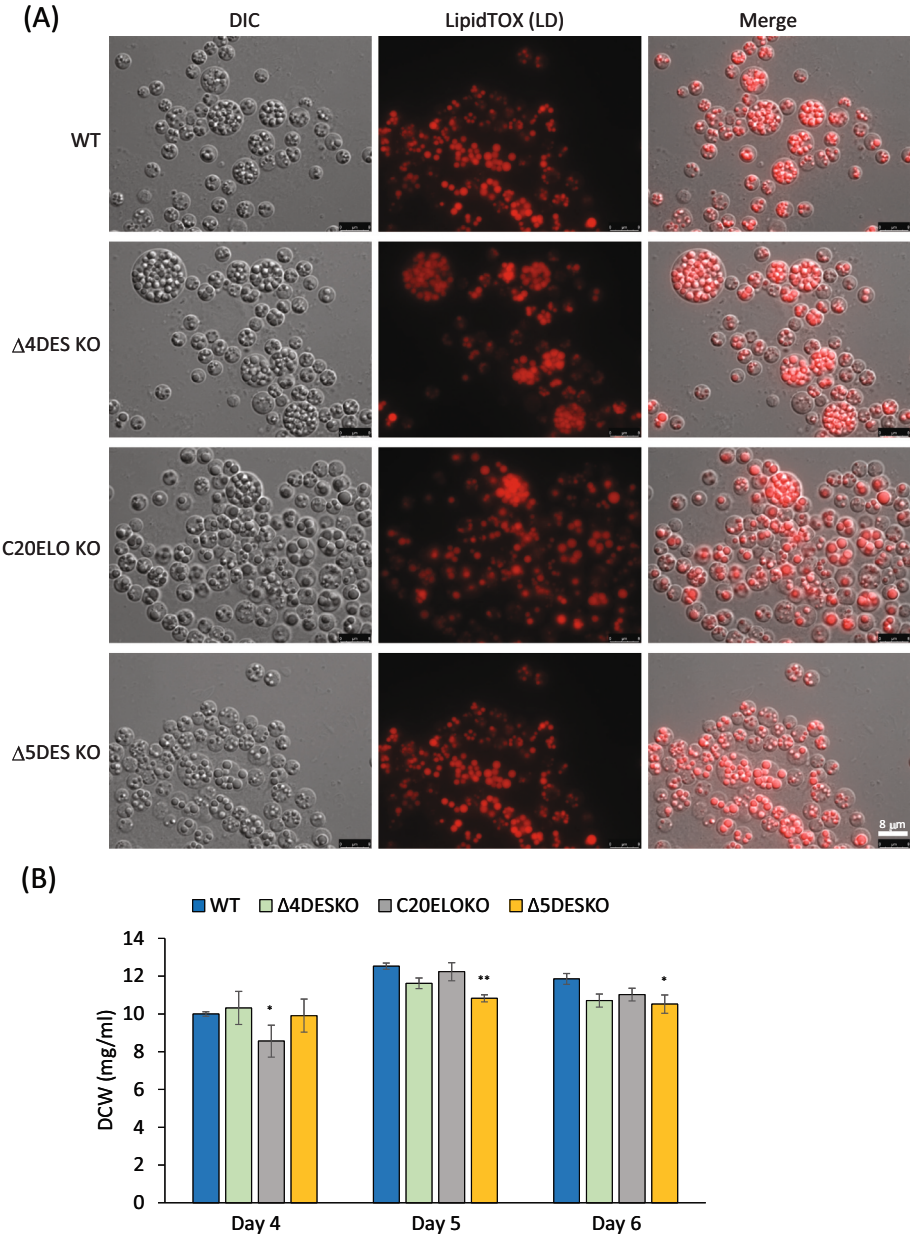

Fig. 4. Lipid droplet and growth characteristics of WT and genome-edited *P. sarkarianum* SEK364 strains
(A) Fluorescence microscopy images showing lipid droplet (LD) formation in WT and genome-edited strains (Δ4DES KO, C20ELO KO, and Δ5DES KO) cultured for 3 days at 25 °C. LipidTOX fluorescence was captured using the Texas Red filter and merged with differential interference contrast (DIC) images. Scale bar represents 8 μm. (C) Dry cell weight (DCW) per 1 mL of culture for WT and genome-edited strains cultured at 25 °C. Samples were collected daily from day 4 to day 6, and the dry weight of lyophilized samples was measured. Statistical significance compared to WT was assessed by one-way ANOVA, and the results are shown on the graphs. Data are presented as mean ± SD ($n = 3$).

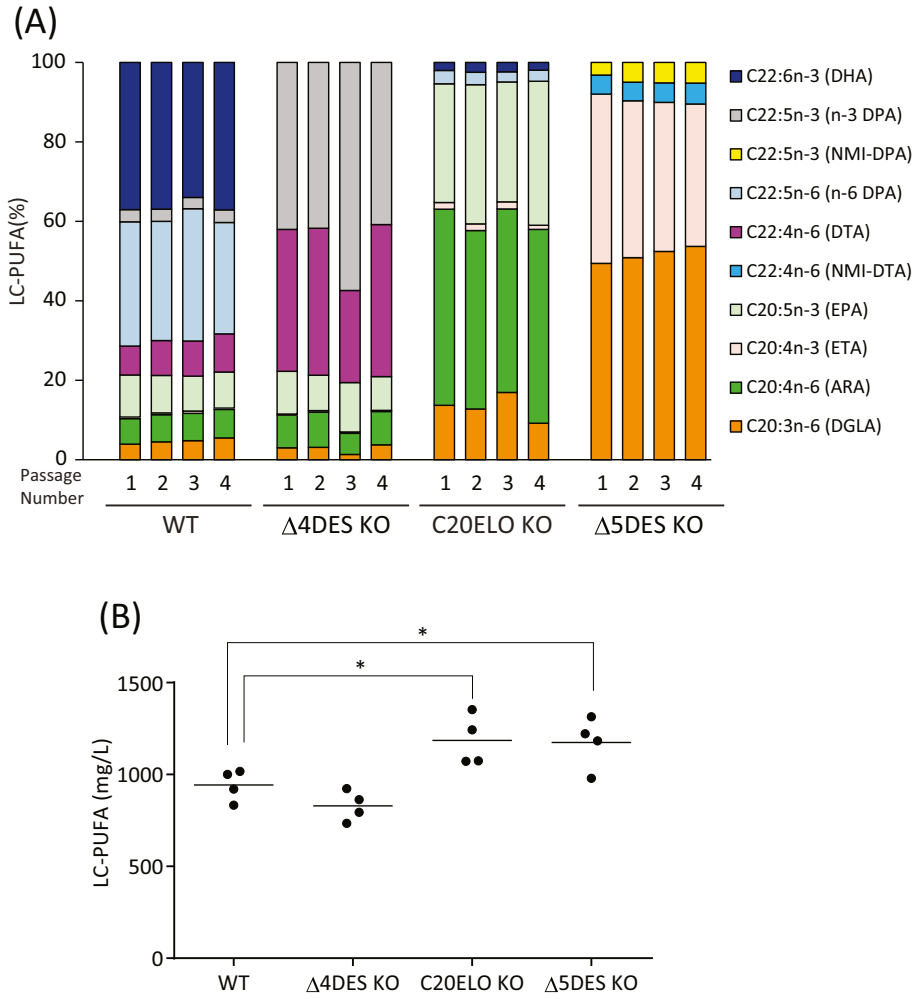

Fig. 5. Assessment of the stability of LC-PUFA composition and productivity in genome-edited *P. sarkarianum* SEK364 strains after repeated passages
(A) Stability of LC-PUFA composition during serial subculturing of WT and genome-edited strains (Δ4DES KO, C20ELO KO, and Δ5DES KO). WT and each genome-edited strain were subcultured every 4 days in 3 mL of GY medium. At each passage, 1 mL of culture was collected for GC analysis of LC-PUFA composition. The LC-PUFA species are indicated in the footnote on the right. (B) LC-PUFA productivity (mg/L) of WT and genome-edited strains across four passages. The total LC-PUFA content was plotted for each passage, with horizontal lines representing mean values. Statistical significance relative to WT was determined by one-way ANOVA.

revealed that productivity remained stable across successive passages, indicating that both composition and LC-PUFA yield were unaffected by repeated cultivation (Fig. 5B). Notably, LC-PUFA productivity was significantly higher in the C20ELO KO and Δ5DES KO strains compared to WT (Fig. 5B), whereas no significant difference was observed between WT and the Δ4DES KO strain (Fig. 5B).

3.9. mRNA expression analysis of ELO/DES pathway genes in WT and genome-edited P. sarkarianum SEK364 strains

Given the disruption of metabolic enzyme genes in the ELO/DES pathway, we hypothesized that compensatory mechanisms might be activated. Moreover, the observed increase in LC-PUFA productivity in the C20ELO KO and Δ5DES KO strains prompted us to investigate the underlying cause. To this end, RNA was extracted from WT and genome-edited strains, and the expression levels of ELO/DES pathway genes were quantified by qPCR (Fig. 6). Using *S. cerevisiae* genes as queries, three universally conserved eukaryotic housekeeping genes, EF1α, β-tubulin, and β-actin, were identified from the draft genome of *P. sarkarianum* [23] and employed as reference genes for qPCR normalization. qPCR results confirmed the absence of amplification curves for the targeted genes in each genome-edited strain, verifying successful knockout as expected (Fig. 6). In the C20ELO KO strain, expression of C18ELO, which partially compensate for C20ELO function, and upstream elongase C16ELO were significantly upregulated (Fig. 6). Similarly, in the Δ5DES KO strain, expression of C20ELO, critical for the synthesis of NMI-DTA and NMI-DPA, was markedly increased (Fig. 6). Notably, both C20ELO KO and Δ5DES KO strains, which exhibited enhanced LC-PUFA productivity (Fig. 5B), showed overall upregulation of pathway genes, suggesting that transcriptional compensation contributes to improved productivity (Fig. 6). In contrast, the Δ4DES KO strain displayed no significant differences in expression compared to WT (Fig. 6). Both C20ELO KO and Δ5DES KO strains exhibited reduced proportions of C22-chain PUFAs relative to WT and Δ4DES KO strains (Fig. 2H, Fig. 5A). These findings imply that C22 LC-PUFAs such as DHA (C22:6) and DPA (C22:5) are important for the survival and growth of *P. sarkarianum* SEK364, and that the organism senses their depletion and activates compensatory mechanisms to promote their synthesis.

3.10. Optimization of culture conditions for enhancing the productivity of LC-PUFAs of genome-edited P. sarkarianum SEK364 strains

The Δ5DES KO strain of *P. sarkarianum* established in this study represents the first successful knockout of the Δ5 desaturase gene in this species. Because the productivity of key LC-PUFAs such as DGLA and ETA in this strain remains unknown, we sought to identify cultivation

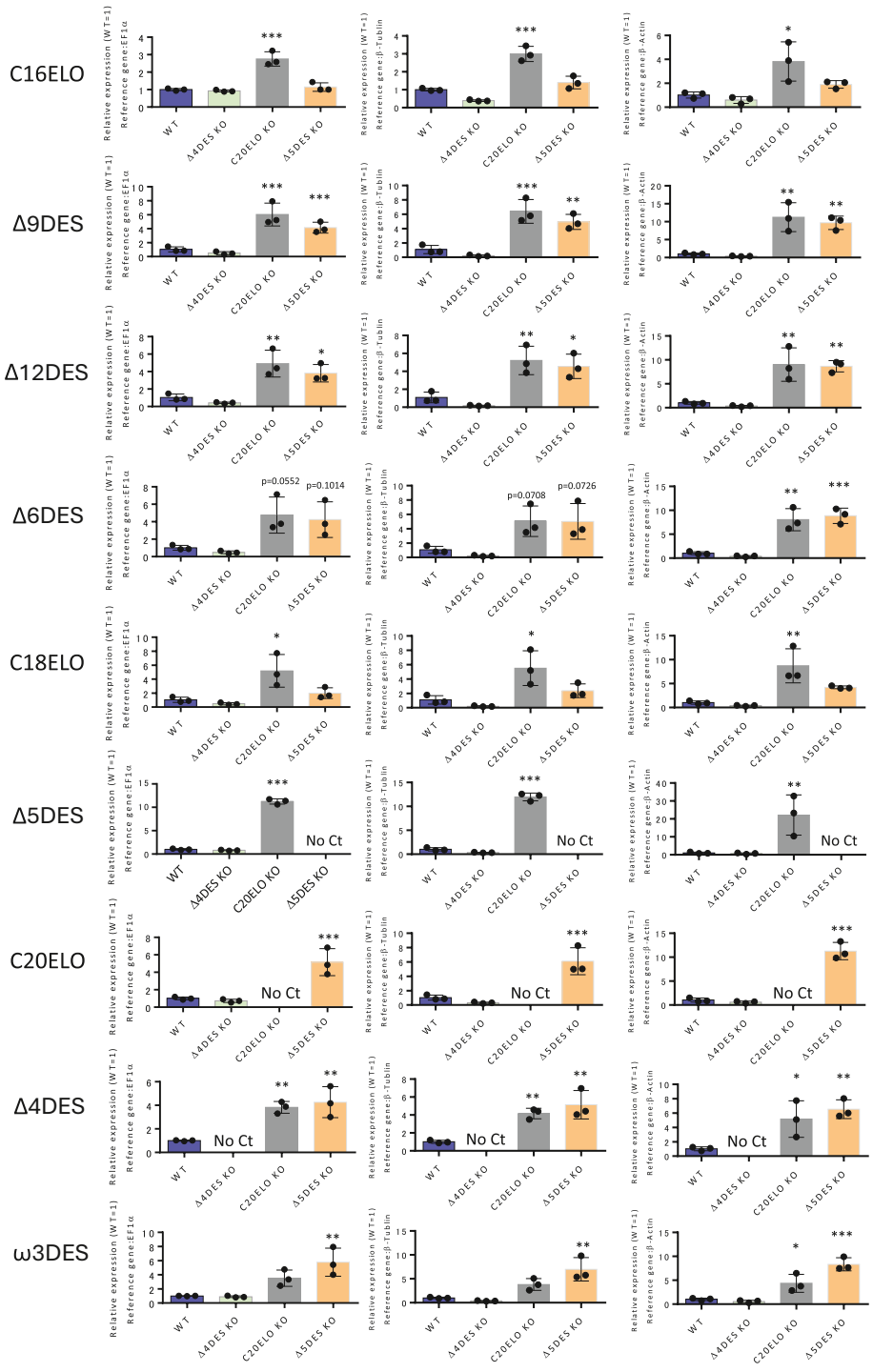

Fig. 6. mRNA expression levels of ELO/DES pathway genes in WT and genome-edited *P. sarkarianum* SEK364 strains
Relative expression of ELO/DES pathway genes was analyzed in WT, Δ4DES KO, C20ELO KO, and Δ5DES KO strains. Gene names are listed on the left side of the figure. Expression levels were calculated by qPCR using the ΔΔCt method, corrected for PCR amplification efficiency, and normalized to WT. Three reference genes were used: Elongation factor 1α (EF1α) (left panel), β-Tubulin (center panel), and β-Actin (right panel). For target genes in genome-edited strains where no amplification curve was detected, "No Ct" is indicated on the graph. Statistical significance compared to WT was assessed by one-way ANOVA, and the results are shown on the graphs. Data are presented as mean ± SD (n = 3).

conditions that maximize their production. The biosynthesis of DGLA from palmitic acid requires three desaturation steps catalyzed by Δ9DES, Δ12DES, and Δ6DES (Fig. 2A). As desaturase enzymes require oxygen for their activity [47], we evaluated the effect of oxygen availability on fatty acid composition by using two types of culture plugs with different levels of aeration: aluminum foil and air-permeable silicone rubber plug (SILICOSEN). As a result, the use of SILICOSEN significantly increased the DGLA ratio by 2-fold compared to aluminum foil (Fig. 7A). Thraustochytrids such as *Aurantiochytrium*, *Thraustochytrium*, and *Parietichytrium* are usually cultured in GY medium containing 3 % glucose [31]. We found that DCW nearly doubled when the glucose concentration was increased from 3 % to 6 % (Fig. 7B). Temporal changes in total fatty acid (TFA) content during the cultivation phase near the peak of DCW showed a consistent increase in TFA levels under the 6 % glucose

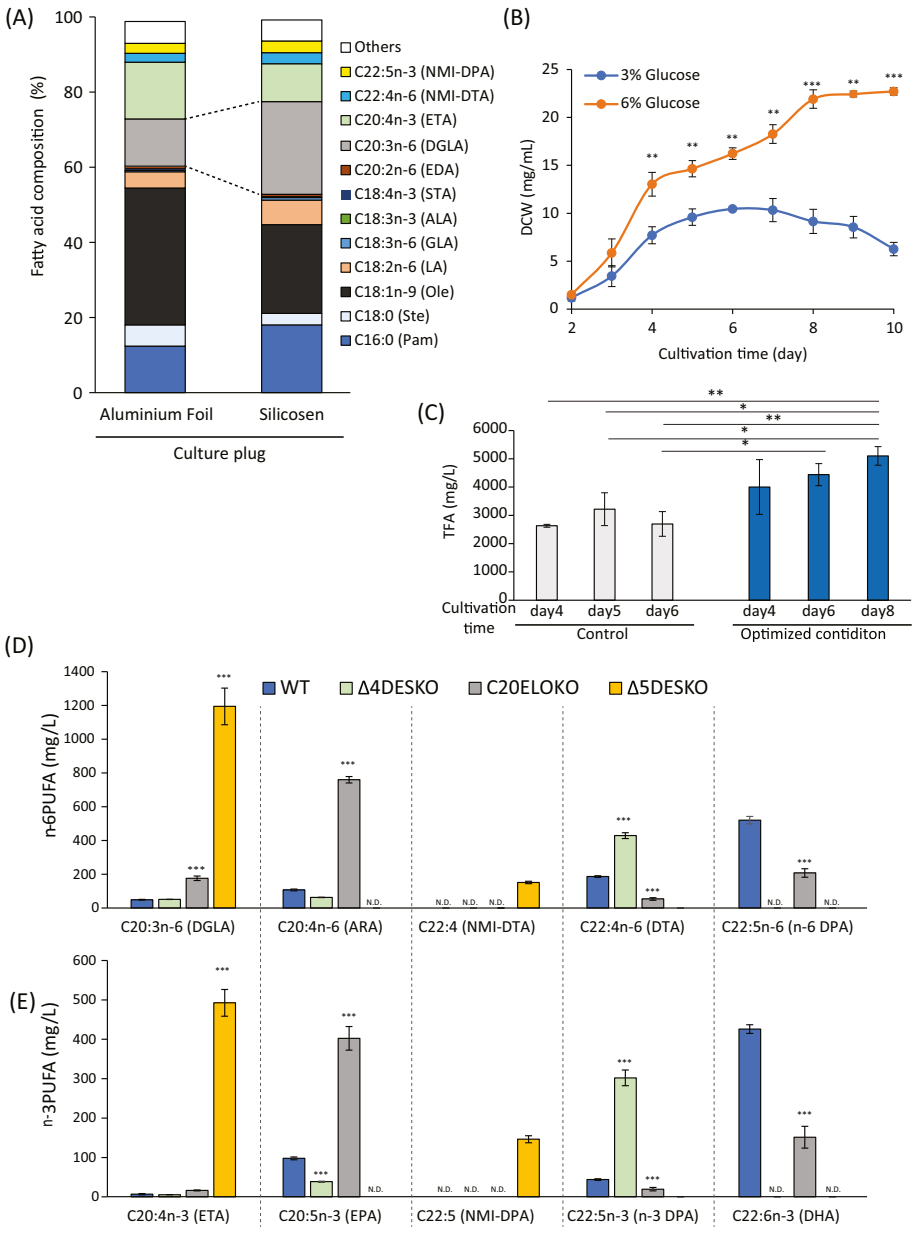

Fig. 7. Evaluation of the effects of different culture conditions and LC-PUFA productivity of genome-edited *P. sarkarianum* SEK364 strains
(A) Effect of two types of plugs with different air permeability on the fatty acid composition of the Δ5DES KO strain. Aluminum foil and SILICOSEN were used as plugs. (B) Evaluation of the effect of glucose concentration in the medium on dry cell weight (DCW) of Δ5DES KO strain. DCW levels were compared between GY media containing 3 % and 6 % glucose. (C) Total fatty acid (TFA) productivity under control conditions (aluminum foil and 3 % glucose) and optimized conditions (SILICOSEN and 6 % glucose). Productivity of n-6 LC-PUFAs (D) and n-3 LC-PUFAs (E). FAMEs were prepared from WT and genome-edited strains (Δ4DES KO, C20ELO KO, and Δ5DES KO) cultured under optimized conditions at 25 °C for 8 days. Statistical significance was assessed by one-way ANOVA, and the results are shown on the graphs. Values below the detection limit are shown as "Not detected (N.D.). Data are presented as Mean ± SD (n = 3).

condition across all examined time points (Fig. 7C). On the other hand, high glucose concentrations did not enhance the proportion of DGLA (Supplemental Fig. 7A), and the use of plugs with different oxygen permeability had little effect on DCW (Supplemental Fig. 7B). Given that both aeration conditions and glucose concentration improved the DGLA ratio and total fatty acid production, we evaluated the combined effects on DGLA productivity of Δ5DES KO strain. Consequently, DGLA was obtained at a high yield exceeding 1 g per liter of culture (Fig. 7D). EPA, DTA, n-3DPA, n-6DPA, and DHA were completely lost in Δ5DES KO strain (Fig. 7D, E). Meanwhile, the Δ5DES KO strain exhibited a remarkable increase in DGLA (1194.5 mg/L) and ETA (492.5 mg/L) levels rising 24.4-fold and 71.3-fold, respectively, compared to the WT. NMI-DTA and NMI-DPA were synthesized only in the Δ5DES KO strain. NMI-DTA reached 151.6 mg/L and NMI-DPA reached 108.5 mg/L, which are comparable to the levels observed in WT for DTA (186.7 mg/L) and EPA (97.9 mg/L) (Fig. 7D, E). The major n-6 LC-PUFA of *P. sarkarianum* SEK364 WT is n-6DPA (520.6 mg/L), and the levels of DGLA, ARA, and DTA are relatively low (Fig. 7D). In WT strain, the primary n-3 LC-PUFA is DHA (425.9 mg/L), while the production levels of ETA, EPA, and n-3DPA remain lower (Fig. 7E). On the other hand, disruption of Δ4DES resulted in marked accumulation of DTA and n-3DPA, with complete loss of n-6DPA and DHA (Fig. 7D, E). The Δ4DES KO strain exhibited a 6.9-fold increase in n-3DPA (302.1 mg/L) and a 2.3-fold increase in DTA (429 mg/L) production compared to the WT (Fig. 7D, E). Disruption of the C20ELO significantly reduced n-6DPA and DHA levels, while concurrently elevating ARA and EPA productivities

(Fig. 7D, E). The C20ELO KO strain exhibited a 7.1-fold increase in ARA (760.2 mg/L) production and a 4.1-fold elevation in EPA (402.4 mg/L) compared to the WT.

In contrast to n-6 LC-PUFAs such as DGLA and ARA, the productivity of n-3 LC-PUFAs including EPA, ETA, and n-3DPA was lower (Fig. 7D, E). Therefore, we investigated cultivation conditions that might enhance the production of n-3 LC-PUFAs. Previous studies on thraustochytrids have shown that cultivation at low temperatures enhances the proportion of n-3 LC-PUFA production [48–52]. In this study, we investigated whether cultivation temperature similarly affects the synthesis of n-3 LC-PUFAs in the *P. sarkarianum* SEK364 WT strain. We compared the standard cultivation temperature of 25 °C with a lower temperature condition of 18 °C and first evaluated the impact on cell growth. Growth rates were calculated based on turbidity measurements at OD_{600} and glucose consumption, the primary carbon source in the medium. In GY medium containing 3 % glucose, the culture at 25 °C reached its maximum growth between days 4 and 5, whereas under low-temperature conditions (18 °C), the maximum was observed between days 6 and 7. These results indicated that the growth of *P. sarkarianum* SEK364 WT strain was delayed under low-temperature conditions (Fig. 8A, B). FAMEs were prepared from samples collected at the time points of maximum growth, day 4 at 25 °C and day 7 at 18 °C, and analyzed by GC to quantify the synthesis of n-3 and n-6 LC-PUFAs. The result demonstrated that *P. sarkarianum* SEK364 WT strain grown at 18 °C exhibited higher production of n-3 LC-PUFAs compared to those grown at 25 °C (Fig. 8C). These findings suggest that the production of n-3 LC-PUFAs in *P. sarkarianum* SEK364 could be enhanced by lower cultivation temperatures, similar to other thraustochytrids. Next, we

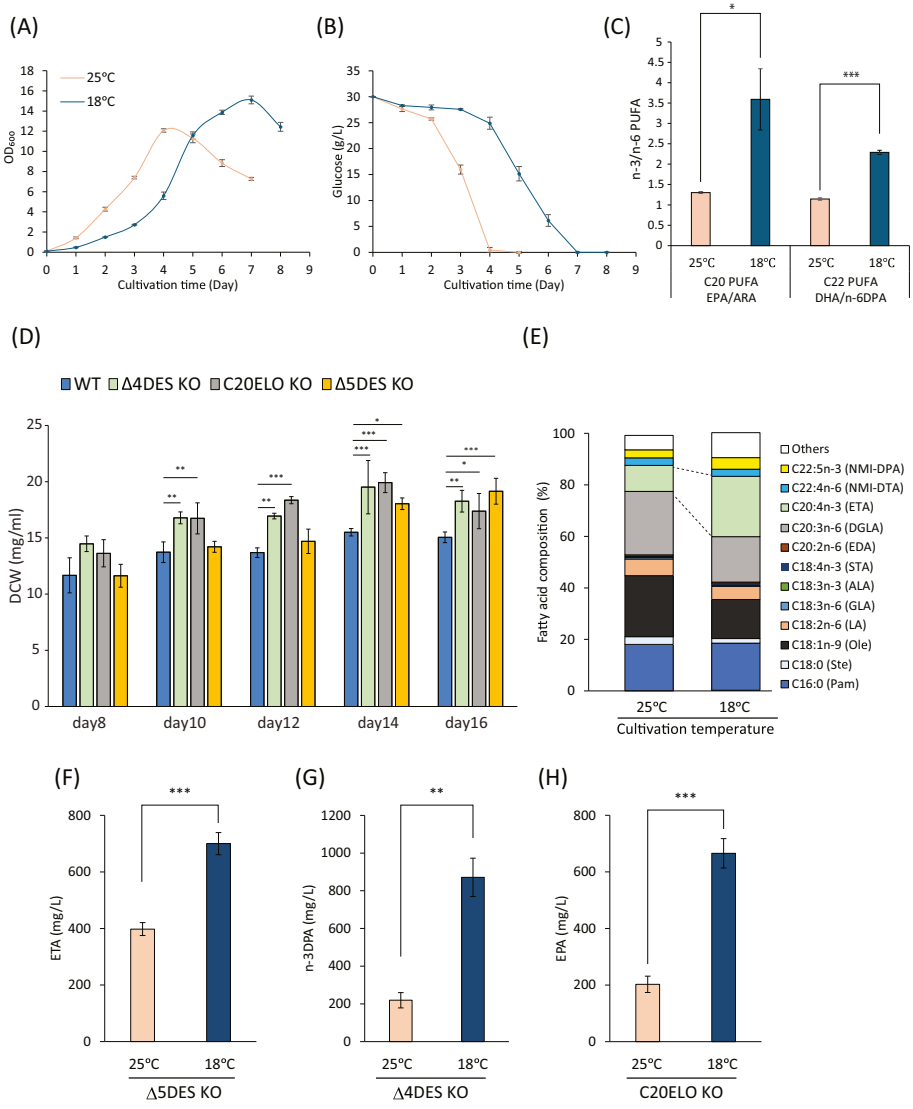

Fig. 8. Effect of cultivation temperature on the growth and n-3 LC-PUFA productivity in *P. sarkarianum* SEK364 WT and genome-edited strains.
(A) Growth curves for 25 °C and 18 °C culture of *P. sarkarianum* SEK364 WT strain. OD_{600} showing turbidity of each cultivation time was measured by spectrophotometer. (B) Glucose consumption rates of 25 °C and 18 °C culture of *P. sarkarianum* SEK364 WT strain. (C) The ratio of n-3 to n-6 LC-PUFA synthesis in WT cultured at 25 °C and 18 °C. FAMEs were prepared from samples that were cultured for 4 days at 25 °C and for 7 days at 18 °C. The EPA (C20:5n-3)/ARA (C20:4n-6) ratio, and DHA (C22:6n-3)/n-6DPA (C22:5n-6) ratio were determined by peak areas obtained by GC analysis. (D) Dry cell weight (DCW) per 1 mL of culture volume for WT and genome-edited strains, which were cultured in GY medium containing 6 % glucose at 18 °C. Culture samples were collected every two days from day 8 to day 16 and their dry weight was measured after lyophilization. Statistical significance was assessed by one-way ANOVA. (E) Effect of cultivation temperature on the fatty acid composition of the Δ5DES KO strain. (F) ETA productivity of Δ5DES KO strain cultured at 25 °C and 18 °C. (G) n-3DPA productivity of Δ4DES KO strain cultured at 25 °C and 18 °C. (H) EPA productivity of C20ELO KO strain cultured at 25 °C and 18 °C. FAMEs were prepared from cells that were cultured in GY medium (3 % glucose) at 25 °C for 6 days, or GY medium (6 % glucose) at 18 °C for 14 days. Statistical significance was assessed by an unpaired, two-tailed Student's *t*-test, and the results are shown on the graphs. Data are presented as Mean ± SD (n = 3).

cultured the *P. sarkarianum* SEK364 WT and genome edited strains (Δ4DES KO, C20ELO KO, and Δ5DES KO) in 6 % glucose medium, which could promote lipid production (Fig. 7), under low-temperature conditions (18 °C). We found that none of the genome-edited strains exhibited growth defects or abnormal LD formation compared to the WT (Fig. 8D, Supplemental Fig. 8). Fatty acid profiling of the Δ5DES KO strain cultured at 18 °C revealed an increase in ETA levels accompanied by a reduction in DGLA (Fig. 8E). Notably, the Δ5DES KO strain cultivated at 18 °C exhibited the highest ETA production, reaching 700 mg/L (Fig. 8F). Similarly, increased levels of n-3DPA (871. 6 mg/L) and EPA (665.8 mg/L) were also observed in the Δ4DES KO and C20ELO KO strains cultured at 18 °C (Fig. 8G, H). Taken together, these findings demonstrate that although low-temperature cultivation leads to slower growth and a prolonged time to reach peak DCW, it significantly enhances the production of target n-3 LC-PUFAs.

4. Discussion

Most microorganisms used for host lack the ability to synthesize LC-PUFAs; therefore, enabling LC-PUFA production typically requires the introduction of multiple exogenous genes, representing an "additive" genetic modification [53]. In contrast, *P. sarkarianum* SEK364 used in this study, possesses a complete biosynthetic pathway from palmitic acid (C16:0) to DHA (C22:6) (Fig. 2A). This study demonstrated that targeted gene deletions using transgene-free genome editing, representing a "subtractive" approach, allow precise modulation of LC-PUFA composition. To the best of our knowledge, this is the first study in oleaginous microorganisms to achieve flexible remodeling of LC-PUFA composition by disrupting genes in the ELO/DES pathway through genome editing.

CRISPR/Cas9-mediated genome editing in *Aurantiochytrium* had been reported in a previous study, wherein exogenous antibiotic resistance genes were employed as donor marker to isolate genome-edited strain [28] or to express Cas9 and gRNA [29]. In this study, we developed a method that enables the generation of genome-edited strains through direct RNP delivery without relying on exogenous selection markers in three phylogenetically distinct genera of thraustochytrids, namely *Aurantiochytrium, Thraustochytrium* and *Parietichytrium*, suggesting its broad applicability across the thraustochytrid. By exclusively employing RNPs for gene modification, the resulting genome-edited thraustochytrids circumvent the various restrictions typically associated with GMOs in many countries [27]. Furthermore, the genome-edited strains established in this study demonstrated a high production of the target LC-PUFAs. To date, oleaginous microorganisms such as *Mortierella alpina* and *Yarrowia lipolytica* have been reported as sources for fermentative DGLA production, with reported yields of 884 mg/L and 832 mg/L in flask cultures, respectively [54,55]. Notably, the DGLA production in flask culture of our Δ5DES KO strain exceeds these values (1195 mg/L), making it the most promising source for DGLA production (Fig. 5D). The Δ5DES KO strain produces ETA in addition to DGLA (Fig. 4B). ETA (C20:4n-3) is expected to exhibit significant bioactive properties because of its structural similarity to ARA (C20:4n-6) and EPA (C20:5n-3). However, due to its scarcity in natural sources, its physiological functions remain largely unknown. To elucidate the biological activities of ETA, and to facilitate application in medical and nutritional fields, the development of a stable supplying system is required. Previous studies have attempted ETA production in the oleaginous filamentous fungus *Mucor circinelloides* by introducing heterologous elongase and ω3 desaturase genes via genetic modification, resulting in a yield of 115 mg/L after 4 days of cultivation [56]. A genetically modified *M. alpina* mutant expressing a heterologous ω3 desaturase was reported to produce approximately 600 mg/L of ETA after 10 days of cultivation [57]. In this study, we found that culturing the Δ5DES KO strain under low-temperature condition (18 °C) resulted in the production of 700 mg/L of ETA (Fig. 6F), indicating that Δ5DES KO strain possesses considerable potential as a microbial platform for ETA production. In a previous study, high LC-PUFA productivity was achieved using a jar fermenter, yielding 11.4 g/L of EPA in the C20ELO KO strain and 4.8 g/L of n-3 DPA in the Δ4DES KO strain of *Parietichytrium* [23]. Thus, further optimization of the jar fermenter culture is expected to improve the productivity of DGLA and ETA of Δ5DES KO strain.

Some conifer seeds, such as pine nut oil, are known to contain NMI-PUFAs including pinolenic acid (cis-5,9,12-Octadecatrienoic acid) and sciadonic acid [58]. Studies using animal models have suggested that these NMI-PUFAs may exert beneficial effects on lipid metabolic disorders and functional impairments in liver associated with obesity [58,59]. In this study, we identified a novel NMI-PUFA, designated as NMI-DPA (Fig. 3). Unlike methylene-interrupted LC-PUFAs such as n-3DPA and n-6DPA, NMI-DPA may possess distinct biological functions and potential health benefits. However, the production yields of NMI-DTA and NMI-DPA were considerably lower than that of DGLA or ETA (Fig. 7D, E), making it currently difficult to obtain sufficient quantities for functional evaluation. Substrate specificity analysis of C20ELO using *S. cerevisiae* revealed that C20ELO from *P. sarkarianum* can utilize DGLA as a substrate (Supplemental Fig. 6). In mammals, ELOVL2 and ELOVL5 are known to catalyze the elongation of LC-PUFAs from C20 to C22, and previous studies have reported that these enzymes act on ARA or EPA following Δ5-desaturation by FADS1 [60]. However, to the best of our knowledge, no reports exist of ELOVL2/5 acting directly on LC-PUFAs such as DGLA or ETA that have not undergone Δ5-desaturation, suggesting that our findings represent the first evidence of such activity. Notably, the higher abundance of DGLA compared to NMI-DTA implies that ARA may serve as a more favorable substrate (Fig. 7D). Consistent with this, the conversion efficiency from ARA (C20:4) to DTA (C22:4) was higher than that from DGLA (C20:3) to DtriA (C22:3) (Supplemental Fig. 6E). These results indicate that C20ELO recognizes Δ5-desaturation and that this structural feature influences its catalytic activity. Future studies aimed at elucidating the molecular basis of this substrate specificity and engineering variants with enhanced preference for DGLA could enable the development of strains with improved NMI-PUFA production.

Low-temperature cultivation increased the proportion of n-3 LC-PUFA not only in the Δ5DES KO strain, but also in the *P. sarkarianum* SEK364 WT, as well as in the Δ4DES KO and C20ELO KO strains. Some psychrophilic marine bacteria are known to promote the synthesis of n-3 LC-PUFAs with low melting points, enabling the maintenance of membrane fluidity under cold conditions [61]. An increase in the proportion of n-3 LC-PUFAs at lower temperatures is considered one of the adaptive mechanisms by which *P. sarkarianum* SEK364 responds to environmental changes. Importantly, both *Aurantiochytrium* and *Parietichytrium*, which employ distinct biosynthetic pathways for DHA [23,62], show increased n-3 LC-PUFA production under low-temperature cultivation [50,51]. These findings imply the involvement of a conserved mechanism shared among thraustochytrids, independent of the DHA biosynthetic pathways. Elucidating the mechanisms underlying the enhanced synthesis of n-3 LC-PUFAs at lower cultivation temperatures remains a critical subject for future investigation.

In mammals, FADS2, the Δ6DES, is an enzyme involved in LC-PUFA biosynthesis. Its mRNA expression has been suggested to be negatively regulated by DHA, via the peroxisome proliferator–activated receptor α (PPARα) and retinoid X receptor α (RXRα) [63]. In Atlantic salmon, CRISPR/Cas9-mediated disruption of *elovl2*, which functions as the C20ELO, has been reported to enhance the expression of LC-PUFA biosynthetic genes through sterol regulatory element–binding protein-1 (SREBP-1) [64]. Together, these observations support a model in which sufficient DHA constrains its own synthesis through the PPARα–RXRα axis, whereas DHA deficiency due to impaired synthesis triggers compensatory upregulation of LC-PUFA biosynthesis via SREBP-1. Consistent with this framework, our qPCR analysis of mRNA levels for all enzymes in the ELO/DES pathway revealed both the C20ELO KO and Δ5DES KO exhibited broadly elevated expression of LC-PUFA

biosynthetic genes (Fig. 6). These findings suggest that *P. sarkarianum* SEK364 harbors a regulatory system that senses C22 LC-PUFAs and accordingly modulates their biosynthesis, functionally analogous to the PPARα–RXRα and SREBP-1 circuits described in vertebrates. Notably, canonical PPARα, RXRα, and SREBP-1 homologs are not detected in the draft genome of *P. sarkarianum* SEK364 [23], implying the presence of a specific regulatory mechanism in *P. sarkarianum* or, more broadly, in thraustochytrids.

The genome editing method developed in this study will be widely applicable in thraustochytrid research from basic to applied studies. Thus, we discuss the concerns regarding efficiency and off-target in the following sections. In this study, we established three genome-edited strains of *P. sarkarianum* SEK364. However, the efficiency varied depending on the target gene (Δ4DES KO: 4/280 colonies (1.4 %), C20ELO KO: 1/196 colonies, (0.6 %), Δ5DES hKO:1/528 colonies (0.2 %), and Δ5DES KO:1/288 colonies (0.35 %)). To screen genome-edited strains, we employed agarose gel electrophoresis to detect size shifts in PCR products resulting from dual cleavage within the target gene. This method is advantageous because it requires minimal procedures, no need for heteroduplex formation and making PAGE gels, and enables rapid, high-throughput screening of large numbers of samples. One limitation of our screening strategy is that genome-edited strains may have been overlooked when cleavage occurred at only one of the two intended sites. As shown in Fig. 1F, even with two crRNAs, approximately half of the samples exhibited cleavage at a single site rather than both. Because our detection relied on identifying edits at both sites, strains with single-site modifications were not counted as successful edits. This suggests that the calculated editing efficiency likely underestimates the true frequency of genome modification. In practice, the actual efficiency may be higher, highlighting the need for alternative validation approaches that can capture single-site edits and provide a more accurate assessment of editing performance.

The results of color selection targeting the *GUS* gene in *A. limacinum* ATCC MYA-1381 and *T. aureum* ATCC 34304, which employed a single crRNA, are considered to more accurately reflect RNP-based genome editing efficiency for thraustochytrids. Despite using the same target gene, crRNA, and delivery conditions, genome editing efficiency for the GUS gene in *A. limacinum* ATCC MYA-1381 and *T. aureum* ATCC 34304 varied substantially (Fig. 1D), indicating that the physiological state of the cells at the time of RNP delivery strongly influences genome-editing outcomes. In *P. sarkarianum* SEK364, three metabolic enzyme genes were targeted; however, it remains unresolved whether the observed variation reflects gene-specific effects or stems from methodological variability. To identify conditions that promote an optimal cellular state, we systematically evaluated multiple parameters prior to RNP delivery, including pre- and main-culture durations, glucose concentration, carbon source, and washing conditions, with the aim of enhancing and standardizing editing efficiency. Nevertheless, no combination of conditions consistently produced reliable genome editing outcomes. Although the RNP-based genome editing approach presented here shows variability in efficiency, it is noteworthy that at least one genome-edited strain was obtained under every experimental condition across *A. limacinum* ATCC MTA-1381, *T. aureum* ATCC 34304, and *P. sarkarianum* SEK364. This suggests that, with access to a high-throughput screening strategy, such as capillary or microchip electrophoresis are available [44], isolating the desired genome-edited strains should not pose a major challenge, making this approach a practical option for genome editing in thraustochytrids.

The transient induction of Cas9 as RNP could ensure that Cas9 is not constitutively expressed in thraustochytrids. This transient Cas9 contributes to reducing the risk of off-target effects [26]. Notably, the genome-edited strains generated in this study were largely comparable to the WT in terms of growth and lipid droplet development under both 25 °C and 18 °C culture conditions (Fig. 4A and B, Fig. 8D, Supplemental Fig. 8). Additionally, the genome-edited strains did not exhibit any reduction in LC-PUFA productivity compared with the WT; in fact, the C20ELO KO and Δ5DES KO strains showed increased production, concomitant with elevated mRNA expression of metabolic enzyme genes in the ELO/DES pathway (Fig. 5B). These results suggest that, at least for the genome-edited strains established in this study, no off-target effects compromise their utility as LC-PUFA producing microorganisms.

Conventional genetic engineering approaches typically rely on selectable markers, such as antibiotic resistance genes, to isolate successfully transformed cells [31]. However, the limited availability of such markers restricts the number of genetic modifications that can be introduced into a single host. To enhance the productivity of target LC-PUFAs, it is necessary to integrate multiple genetic modifications into one host, which often requires marker recycling, a process involving the removal of markers from the genomic DNA [65]. In contrast, the RNP-based genome editing method presented in this study does not depend on selectable markers, thereby eliminating both the numerical limitations and procedural complexity associated with marker-based selection. This advantage enables more flexible and streamlined genetic manipulation of thraustochytrids. Because this method does not require selectable markers and imposes no limitation on the number of genetic modifications, we plan to integrate multiple gene edits that enhance the productivity of various target LC-PUFAs. In recent years, we have elucidated TG degradation mechanisms in thraustochytrids, including lipophagy, a selective autophagy targeting LD, and a lipase-mediated lipolysis pathway that functions cooperatively with lipophagy [66]. Disrupting these TG degradation pathways through genome editing is expected to enhance the production of target LC-PUFAs. Ultimately, the resulting high-producing strains will undergo whole-genome sequencing to obtain detailed genomic information, which will serve as a foundation for their practical application.

CRediT authorship contribution statement

Yohei Ishibashi: Writing – review & editing, Writing – original draft, Visualization, Project administration, Investigation, Funding acquisition, Data curation, Conceptualization. **Ryuji Tanimura:** Investigation, Data curation. **Yusuke Ataka:** Investigation, Data curation. **Akito Kumagai:** Investigation, Data curation. **Daiske Honda:** Resources. **Makoto Ito:** Writing – review & editing, Supervision, Conceptualization. **Nozomu Okino:** Writing – review & editing, Supervision, Project administration, Funding acquisition.

Grant support

This study was supported in part by a Grant-in-Aid for Challenging Exploratory Research (18K19183), and Grant-in-Aid for Scientific Research (C) (24K08702, 24K09042) from the Japanese Ministry of Education, Culture, Sports, Science, and Technology.

Declaration of competing interest

The authors declare that they have no known competing financial interests or personal relationships that could have appeared to influence the work reported in this paper.

Appendix A. Supplementary data

Supplementary data to this article can be found online at https://doi.org/10.1016/j.cej.2025.171156.

Data availability

All data supporting the findings of this study are available within the article and its supplementary materials. Additional datasets generated and analyzed during the current study are available from the corresponding author upon reasonable request.

References

[1] L.F.C. Castro, D.R. Tocher, O. Monroig, Long-chain polyunsaturated fatty acid biosynthesis in chordates: insights into the evolution of fads and Elovl gene repertoire, Prog. Lipid Res. 62 (2016) 25–40, https://doi.org/10.1016/J.PLIPRES.2016.01.001.

[2] S.C. Dyall, L. Balas, N.G. Bazan, J.T. Brenna, N. Chiang, F. da Costa Souza, J. Dalli, T. Durand, J.M. Galano, P.J. Lein, C.N. Serhan, A.Y. Taha, Polyunsaturated fatty acids and fatty acid-derived lipid mediators: recent advances in the understanding of their biosynthesis, structures, and functions, Prog. Lipid Res. 86 (2022) 101165, https://doi.org/10.1016/J.PLIPRES.2022.101165.

[3] T. Sassa, A. Kihara, Metabolism of very long-chain fatty acids: genes and pathophysiology, Biomol Ther (Seoul) 22 (2014) 83–92, https://doi.org/10.4062/BIOMOLTHER.2014.017.

[4] J.P. SanGiovanni, E. Agrón, A.D. Meleth, G.F. Reed, R.D. Sperduto, T.E. Clemons, E.Y. Chew, Ω–3 Long-chain polyunsaturated fatty acid intake and 12-y incidence of neovascular age-related macular degeneration and central geographic atrophy: AREDS report 30, a prospective cohort study from the age-related eye disease study, Am. J. Clin. Nutr. 90 (2009) 1601–1607, https://doi.org/10.3945/AJCN.2009.27594.

[5] Y. Lee, L. Lee, L. Zhang, Q. Zhou, Association between fatty acid intake and age-related macular degeneration: a meta-analysis, Front. Nutr. 11 (2024) 1403987, https://doi.org/10.3389/FNUT.2024.1403987.

[6] R. Crupi, S. Cuzzocrea, Role of EPA in inflammation: mechanisms, effects, and clinical relevance, Biomolecules 12 (2022) 242, https://doi.org/10.3390/BIOM12020242.

[7] G. Drouin, D. Catheline, E. Guillocheau, P. Gueret, C. Baudry, P. Le Ruyet, V. Rioux, P. Legrand, Comparative effects of dietary n-3 docosapentaenoic acid (DPA), DHA and EPA on plasma lipid parameters, oxidative status and fatty acid tissue composition, J. Nutr. Biochem. 63 (2019) 186–196, https://doi.org/10.1016/J.JNUTBIO.2018.09.029.

[8] M. Phang, L.F. Lincz, M.L. Garg, Eicosapentaenoic and docosahexaenoic acid supplementations reduce platelet aggregation and hemostatic markers differentially in men and women, J. Nutr. 143 (2013) 457–463, https://doi.org/10.3945/JN.112.171249.

[9] X. Fei Guo, A.J. Sinclair, G. Kaur, D. Li, Differential effects of EPA, DPA and DHA on cardio-metabolic risk factors in high-fat diet fed mice, Prostaglandins Leukot. Essent. Fatty Acids 136 (2018) 47–55, https://doi.org/10.1016/J.PLEFA.2017.09.011.

[10] A. Nakamura, S. Sakai, Y. Taketomi, J. Tsuyama, Y. Miki, Y. Hara, N. Arai, Y. Sugiura, H. Kawaji, M. Murakami, T. Shichita, PLA2G2E-mediated lipid metabolism triggers brain-autonomous neural repair after ischemic stroke, Neuron 111 (2023) 2995–3010.e9, https://doi.org/10.1016/J.NEURON.2023.06.024.

[11] K. Tan, H. Zhang, H. Zheng, Climate change and n-3 LC-PUFA availability, Prog. Lipid Res. 86 (2022) 101161, https://doi.org/10.1016/J.PLIPRES.2022.101161.

[12] R. Yokoyama, D. Honda, R. Yokoyama, D. Honda, Taxonomic rearrangement of the genus Schizochytrium sensu lato based on morphology, chemotaxonomic characteristics, and 18S rRNA gene phylogeny (Thraustochytriaceae, Labyrinthulomycetes): emendation for Schizochytrium and erection of Aurantiochytrium and Oblongichytrium gen. Nov, Mycoscience 48 (2007) 199–211, https://doi.org/10.1007/S10267-006-0362-0.

[13] R. Yokoyama, B. Salleh, D. Honda, R. Yokoyama, B. Salleh, D. Honda, Taxonomic rearrangement of the genus Ulkenia sensu lato based on morphology, chemotaxonomical characteristics, and 18S rRNA gene phylogeny (Thraustochytriaceae, Labyrinthulomycetes): emendation for Ulkenia and erection of Botryochytrium, Parietichytrium, and Sicyoidochytrium gen. nov, Mycoscience 48 (2007) 329–341, https://doi.org/10.1007/S10267-007-0377-1.

[14] X. Han, Y. Liu, Y. Yuan, Z. Chen, Metabolic engineering of Schizochytrium sp. for superior docosahexaenoic acid production, Algal Res. 77 (2024) 103355, https://doi.org/10.1016/J.ALGAL.2023.103355.

[15] A.J. Ryu, W.S. Shin, S. Jang, Y. Lin, Y. Park, Y. Choi, J.Y. Kim, N.K. Kang, Enhancing fatty acid and omega-3 production in Schizochytrium sp. using developed safe-harboring expression system, J. Biol. Eng. 18 (2024) 1–11, https://doi.org/10.1186/S13036-024-00447-Y/FIGURES/5.

[16] Y. Liu, X. Han, Z. Chen, Y. Yan, Z. Chen, Selectively superior production of docosahexaenoic acid in Schizochytrium sp. through engineering the fatty acid biosynthetic pathways, Biotechnol. Biofuels Bioprod. 17 (2024) 1–13, https://doi.org/10.1186/S13068-024-02524-2/FIGURES/7.

[17] L. Chen, S. Tong, W. Liu, Y. Zhang, H. Khalid, L. Long, Y. Li, D. Li, B. Yan, G. Chen, Electroporation-induced mutation and transcriptome analysis for high DHA production in Schizochytrium limacinum GCD2032, Algal Res. 76 (2023) 103297, https://doi.org/10.1016/J.ALGAL.2023.103297.

[18] K. Lu, F. Wang, L. Chen, W. Zhang, Overexpression of S-R enhances the accumulation of biomass, fatty acids, and β-carotene in Schizochytrium, Bioresour. Technol. 385 (2023) 129452, https://doi.org/10.1016/J.BIORTECH.2023.129452.

[19] C. Morabito, C. Bournaud, C. Maës, M. Schuler, R. Aiese Cigliano, Y. Dellero, E. Maréchal, A. Amato, F. Rébeillé, The lipid metabolism in thraustochytrids, Prog. Lipid Res. 76 (2019) 101007, https://doi.org/10.1016/J.PLIPRES.2019.101007.

[20] Z.X. Zhang, H.X. Wu, Y.C. Lin, Y.S. Xu, W. Ma, X.M. Sun, H. Huang, Polyketide synthase acyltransferase domain swapping for enhanced EPA recognition and efficient coproduction of EPA and DHA in Schizochytrium sp, J. Agric. Food Chem. 73 (2024) 2461–2470, https://doi.org/10.1021/ACS.JAFC.4C10465.

[21] J.G. Metz, P. Roessler, D. Facciotti, C. Levering, F. Dittrich, M. Lassner, R. Valentine, K. Lardizabal, F. Domergue, A. Yamada, K. Yazawa, V. Knauf, J. Browse, Production of polyunsaturated fatty acids by potyketide synthases in both prokaryotes and eukaryotes, Science 293 (2001) 290–293, https://doi.org/10.1126/SCIENCE.1059593.

[22] S. Hayashi, Y. Satoh, Y. Ogasawara, T. Dairi, Recent advances in functional analysis of polyunsaturated fatty acid synthases, Curr. Opin. Chem. Biol. 59 (2020) 30–36, https://doi.org/10.1016/J.CBPA.2020.04.015.

[23] Y. Ishibashi, H. Goda, R. Hamaguchi, K. Sakaguchi, T. Sekiguchi, Y. Ishiwata, Y. Okita, S. Mochinaga, S. Ikeuchi, T. Mizobuchi, Y. Takao, K. Mori, K. Tashiro, N. Okino, D. Honda, M. Hayashi, M. Ito, PUFA synthase-independent DHA synthesis pathway in Parietichytrium sp. and its modification to produce EPA and n-3DPA, Commun Biol 4 (2021) 1378, https://doi.org/10.1038/s42003-021-02857-w.

[24] A. Ahmad, A. Jamil, N. Munawar, GMOs or non-GMOs? The CRISPR Conundrum, Front. Plant Sci. 14 (2023) 1232938, https://doi.org/10.3389/FPLS.2023.1232938.

[25] M. Jinek, K. Chylinski, I. Fonfara, M. Hauer, J.A. Doudna, E. Charpentier, A programmable dual-RNA-guided DNA endonuclease in adaptive bacterial immunity, Science 337 (2012) 816–821, https://doi.org/10.1126/SCIENCE.1225829.

[26] Y. Zhang, B. Iaffaldano, Y. Qi, CRISPR ribonucleoprotein-mediated genetic engineering in plants, Plant Commun 2 (2021) 100168, https://doi.org/10.1016/J.XPLC.2021.100168.

[27] M. Tachikawa, M. Matsuo, Global regulatory trends of genome editing technology in agriculture and food, Breed. Sci. 74 (2024) 3–10, https://doi.org/10.1270/jsbbs.23046.

[28] K. Watanabe, C.M.T. Perez, T. Kitahori, K. Hata, M. Aoi, H. Takahashi, T. Sakuma, Y. Okamura, Y. Nakashimada, T. Yamamoto, K. Matsuyama, S. Mayuzumi, T. Aki, Improvement of fatty acid productivity of thraustochytrid, Aurantiochytrium sp. by genome editing, J. Biosci. Bioeng. 131 (2021) 373–380, https://doi.org/10.1016/J.JBIOSC.2020.11.013.

[29] Y. Duan, L. Chen, L. Ma, Y. Zhai, Y. Hu, G. Li, G. Chen, D. Li, CRISPR/Cas9-mediated metabolic engineering for enhanced PUFA production in Schizochytrium limacinum, Chem. Eng. J. 517 (2025) 164320, https://doi.org/10.1016/J.CEJ.2025.164320.

[30] R.A. Jefferson, T.A. Kavanagh, M.W. Bevan, GUS fusions: beta-glucuronidase as a sensitive and versatile gene fusion marker in higher plants, EMBO J. 6 (1987) 3901–3907, https://doi.org/10.1002/J.1460-2075.1987.TB02730.X.

[31] K. Sakaguchi, T. Matsuda, T. Kobayashi, J.I. Ohara, R. Hamaguchi, E. Abe, N. Nagano, M. Hayashi, M. Ueda, D. Honda, Y. Okita, Y. Taoka, S. Sugimoto, N. Okino, M. Ito, Versatile transformation system that is applicable to both multiple transgene expression and gene targeting for thraustochytrids, Appl. Environ. Microbiol. 78 (2012) 3193–3202, https://doi.org/10.1128/AEM.07129-11.

[32] Y. Ishibashi, S. Sadamitsu, Y. Fukahori, Y. Yamamoto, R. Tanogashira, T. Watanabe, M. Hayashi, M. Ito, N. Okino, Characterization of thraustochytrid-specific sterol O-acyltransferase: modification of DGAT2-like enzyme to increase the sterol production in Aurantiochytrium limacinum mh0186, Appl. Environ. Microbiol. 89 (2023), https://doi.org/10.1128/AEM.01001-23 e01001-23.

[33] Y. Ishibashi, K. Aoki, N. Okino, M. Hayashi, M. Ito, A thraustochytrid-specific lipase/phospholipase with unique positional specificity contributes to microbial competition and fatty acid acquisition from the environment, Sci. Rep. 9 (2019) 1–17, https://doi.org/10.1038/S41598-019-52854-7.

[34] K. Ichihara, Y. Fukubayashi, Preparation of fatty acid methyl esters for gas-liquid chromatography, J. Lipid Res. 51 (2010) 635–640, https://doi.org/10.1194/jlr.D001065.

[35] E.G. Bligh, W.J. Dyer, A rapid method of total lipid extraction and purification, Can. J. Biochem. Physiol. 37 (1959) 911–917, https://doi.org/10.1139/O59-099.

[36] T.H. Kuo, H.H. Chung, H.Y. Chang, C.W. Lin, M.Y. Wang, T.L. Shen, C.C. Hsu, Deep Lipidomics and molecular imaging of unsaturated lipid isomers: a universal strategy initiated by mCPBA epoxidation, Anal. Chem. 91 (2019) 11905–11915, https://doi.org/10.1021/ACS.ANALCHEM.9B02667.

[37] K. Ikeda, Y. Oike, T. Shimizu, R. Taguchi, Global analysis of triacylglycerols including oxidized molecular species by reverse-phase high resolution LC/ESI-QTOF MS/MS, J. Chromatogr. B 877 (2009) 2639–2647, https://doi.org/10.1016/J.JCHROMB.2009.03.047.

[38] S. Milne, P. Ivanova, J. Forrester, H. Alex Brown, Lipidomics: an analysis of cellular lipids by ESI-MS, Methods 39 (2006) 92–103, https://doi.org/10.1016/J.YMETH.2006.05.014.

[39] T. Metsalu, J. Vilo, ClustVis: a web tool for visualizing clustering of multivariate data using principal component analysis and heatmap, Nucleic Acids Res. 43 (2015) W566–W570, https://doi.org/10.1093/NAR/GKV468.

[40] M.W. Pfaffl, A new mathematical model for relative quantification in real-time RT–PCR, Nucleic Acids Res. 29 (2001) e45, https://doi.org/10.1093/NAR/29.9.E45.

[41] T. Nakahara, T. Yokochi, T. Higashihara, S. Tanaka, T. Yaguchi, D. Honda, Production of docosahexaenoic and docosapentaenoic acids by Schizochytrium sp. isolated from yap islands, JAOCS, J. Am. Oil Chem. Soc. 73 (1996) 1421–1426, https://doi.org/10.1007/BF02523506.

[42] T. Matsuda, K. Sakaguchi, R. Hamaguchi, T. Kobayashi, E. Abe, Y. Hama, M. Hayashi, D. Honda, Y. Okita, S. Sugimoto, N. Okino, M. Ito, Analysis of Δ12-fatty acid desaturase function revealed that two distinct pathways are active for the synthesis of PUFAs in T. Aureum ATCC 34304, J. Lipid Res. 53 (2012) 1210–1222, https://doi.org/10.1194/JLR.M024935.

[43] J. Dehairs, A. Talebi, Y. Cherifi, J.V. Swinnen, CRISP-ID: decoding CRISPR mediated indels by sanger sequencing, Sci. Rep. 6 (2016) 1–5, https://doi.org/10.1038/SREP28973;TECHMETA.

[44] B. Carrington, K. Bishop, R. Sood, A comprehensive review of Indel detection methods for identification of zebrafish knockout mutants generated by genome-editing nucleases, Genes (Basel) 13 (2022) 857, https://doi.org/10.3390/GENES13050857.
[45] B.D. Wallace, A.B. Roberts, R.M. Pollet, J.D. Ingle, K.A. Biernat, S.J. Pellock, M. K. Venkatesh, L. Guthrie, S.K. O'Neal, S.J. Robinson, M. Dollinger, E. Figueroa, S. R. McShane, R.D. Cohen, J. Jin, S.V. Frye, W.C. Zamboni, C. Pepe-Ranney, S. Mani, L. Kelly, M.R. Redinbo, Structure and inhibition of microbiome β-Glucuronidases essential to the alleviation of Cancer drug toxicity, Chem. Biol. 22 (2015) 1238–1249, https://doi.org/10.1016/J.CHEMBIOL.2015.08.005.
[46] W. Stoffel, I. Hammels, B. Jenke, E. Binczek, I. Schmidt-Soltau, S. Brodesser, M. Odenthal, M. Thevis, Obesity resistance and deregulation of lipogenesis in Δ6-fatty acid desaturase (FADS2) deficiency, EMBO Rep. 15 (2014) 110–120, https://doi.org/10.1002/EMBR.201338041.
[47] M. Cerone, T.K. Smith, Desaturases: structural and mechanistic insights into the biosynthesis of unsaturated fatty acids, IUBMB Life 74 (2022) 1036–1051, https://doi.org/10.1002/IUB.2671.
[48] P.K. Bajpai, P. Bajpai, O.P. Ward, Optimization of production of docosahexaenoic acid (DHA) by Thraustochytrium aureum ATCC 34304, J. Am. Oil Chem. Soc. 68 (1991) 509–514, https://doi.org/10.1007/BF02663823.
[49] L. Zhu, X. Zhang, L. Ji, X. Song, C. Kuang, Changes of lipid content and fatty acid composition of Schizochytrium limacinum in response to different temperatures and salinities, Process Biochem. 42 (2007) 210–214, https://doi.org/10.1016/j.procbio.2006.08.002.
[50] F. Hu, A.L. Clevenger, P. Zheng, Q. Huang, Z. Wang, Low-temperature effects on docosahexaenoic acid biosynthesis in Schizochytrium sp. TIO01 and its proposed underlying mechanism, Biotechnol. Biofuels 13 (2020) 1–14, https://doi.org/10.1186/S13068-020-01811-Y.
[51] Z. Ma, Y. Tan, G. Cui, Y. Feng, Q. Cui, X. Song, Transcriptome and gene expression analysis of DHA producer Aurantiochytrium under low temperature conditions, Sci. Rep. 5 (2015) 1–13, https://doi.org/10.1038/SREP14446.
[52] Z. Ma, M. Tian, Y. Tan, G. Cui, Y. Feng, Q. Cui, X. Song, Response mechanism of the docosahexaenoic acid producer Aurantiochytrium under cold stress, Algal Res. 25 (2017) 191–199, https://doi.org/10.1016/J.ALGAL.2017.05.021.
[53] L. Cao, M. Yin, T.Q. Shi, L. Lin, R. Ledesma-Amaro, X.J. Ji, Engineering Yarrowia lipolytica to produce nutritional fatty acids: current status and future perspectives, synth Syst, Biotechnol 7 (2022) 1024–1033, https://doi.org/10.1016/J.SYNBIO.2022.06.002.
[54] H. Kikukawa, E. Sakuradani, A. Ando, T. Okuda, S. Shimizu, J. Ogawa, Microbial production of dihomo-γ-linolenic acid by Δ5-desaturase gene-disruptants of Mortierella alpina 1S-4, J. Biosci. Bioeng. 122 (2016) 22–26, https://doi.org/10.1016/J.JBIOSC.2015.12.007.
[55] J. Wang, X. Yu, K. Wang, L. Lin, H.H. Liu, R. Ledesma-Amaro, X.J. Ji, Reprogramming the fatty acid metabolism of Yarrowia lipolytica to produce the customized omega-6 polyunsaturated fatty acids, Bioresour. Technol. 383 (2023) 129231, https://doi.org/10.1016/J.BIORTECH.2023.129231.
[56] C. Wu, J. Yang, S. Li, W. Shi, F. Xue, Q. Liu, T. Naz, H. Mohamed, Y. Song, Construction of Eicosatetraenoic acid producing cell factory by genetic engineering of Mucor circinelloides, Fermentation 9 (2023) 653, https://doi.org/10.3390/FERMENTATION9070653.
[57] T. Okuda, A. Ando, H. Negoro, H. Kikukawa, T. Sakamoto, E. Sakuradani, S. Shimizu, J. Ogawa, Omega-3 eicosatetraenoic acid production by molecular breeding of the mutant strain S14 derived from Mortierella alpina 1S-4, J. Biosci. Bioeng. 120 (2015) 299–304, https://doi.org/10.1016/J.JBIOSC.2015.01.014.
[58] Y. Endo, K. Tsunokake, I. Ikeda, Effects of non-methylene-interrupted polyunsaturated fatty acid, Sciadonic (all-cis-5,11,14-eicosatrienoic acid) on lipid metabolism in rats, Biosci. Biotechnol. Biochem. 73 (2009) 577–581, https://doi.org/10.1271/BBB.80646.
[59] L. Chen, Q. Jiang, C. Jiang, H. Lu, W. Hu, S. Yu, M. Li, C.P. Tan, Y. Feng, X. Xiang, G. Shen, Sciadonic acid attenuates high-fat diet-induced obesity in mice with alterations in the gut microbiota, Food Funct. 14 (2023) 2870–2880, https://doi.org/10.1039/D2FO02524H.
[60] E. Ferrero, F.M. Vaz, D. Cheillan, A. Brusco, C. Marelli, The ELOVL proteins: very and ultra long-chain fatty acids at the crossroads between metabolic and neurodegenerative disorders, Mol. Genet. Metab. 144 (2025) 109050, https://doi.org/10.1016/J.YMGME.2025.109050.
[61] D.F. Rodrigues, J.M. Tiedje, Coping with our cold planet, Appl. Environ. Microbiol. 74 (2008) 1677–1686, https://doi.org/10.1128/AEM.02000-07.
[62] S.Y. Cheng, Y.J. Chen, H.C. Lin, H.Y. Chang, M. Der Huang, Genetic analysis of polyunsaturated fatty acids biosynthesis pathway determines four distinct Thraustochytrid types, Environ. Microbiol. 27 (2025) e70090, https://doi.org/10.1111/1462-2920.70090.
[63] D. Majou, Synthesis of DHA (omega-3 fatty acid): FADS2 gene polymorphisms and regulation by PPARα, OCL 28 (2021) 43, https://doi.org/10.1051/OCL/2021030.
[64] A.K. Datsomor, N. Zic, K. Li, R.E. Olsen, Y. Jin, J.O. Vik, R.B. Edvardsen, F. Grammes, A. Wargelius, P. Winge, CRISPR/Cas9-mediated ablation of elovl2 in Atlantic salmon (Salmo salar L.) inhibits elongation of polyunsaturated fatty acids and induces Srebp-1 and target genes, Sci. Rep. 9 (2019) 1–13, https://doi.org/10.1038/S41598-019-43862-8;TECHMETA.
[65] J. Verruto, K. Francis, Y. Wang, M.C. Low, J. Greiner, S. Tacke, F. Kuzminov, W. Lambert, J. McCarren, I. Ajjawi, N. Bauman, R. Kalb, G. Hannum, E. R. Moellering, Unrestrained markerless trait stacking in Nannochloropsis gaditana through combined genome editing and marker recycling technologies, Proc. Natl. Acad. Sci. USA 115 (2018) E7015–E7022, https://doi.org/10.1073/PNAS.1718193115.
[66] S. Wu, Y. Ishibashi, M. Hayashi, N. Okino, Lipid droplet degradation through lipophagy in Aurantiochytrium limacinum mh0186, Mar. Biotechnol. 27 (2025) 1–16, https://doi.org/10.1007/S10126-025-10495-0/METRICS.